

THESIS FOR THE DEGREE OF DOCTOR OF PHILOSOPHY

**MOLECULAR STRUCTURE, INTERACTIONS,  
AND DYNAMICS OF NOVEL LI-BATTERY  
ELECTROLYTES**

LUIS AGUILERA



**CHALMERS**

Department of Physics

Chalmers University of Technology

Göteborg, Sweden 2016

MOLECULAR STRUCTURE, INTERACTIONS, AND DYNAMICS  
OF NOVEL LI-BATTERY ELECTROLYTES

LUIS AGUILERA  
ISBN 978-91-7597-435-4

©LUIS AGUILERA, 2016

Doktorsavhandlingar vid Chalmers tekniska högskola  
Ny serie nr 4116  
ISSN 0346-718X

Department of Physics  
Chalmers University of Technology  
SE-412 96 Göteborg  
Sweden  
Telephone + 46 (0)31-772 1000

Chalmers Reproservice  
Göteborg, Sweden 2016

# **Molecular structure, interactions, and dynamics of novel Li-battery electrolytes**

LUIS AGUILERA

Department of Physics, Chalmers University of Technology

## **Abstract**

Lithium-ion batteries are one of the most promising candidates for energy storage in sustainable technologies such as electro-mobility or renewable energy systems. However, at present they are incapable to compete with the combustion engine to power vehicles in terms of capacity, price, and safety. The same shortcomings are also limiting the applicability in large-scale grid energy storage. A key component for improved performance is the electrolyte where a better understanding of the limiting mechanism at a molecular level is needed in order to achieve beyond state-of-the-art technology.

This thesis focuses on understanding new types of electrolytes from structural and dynamical points of view. While the commonly used electrolytes consist of a mixture of organic solvents and moderate concentrations of lithium salts, recent studies suggest the use of super-concentrated electrolytes or the implementation of ionic liquids, as additives or as full replacement of the organic solvent, as promising development routes. A common feature of these new electrolytes is a complex structure with characteristic length scales exceeding those normally found in simple liquids. Due to their ionic nature and surfactant-like structure ionic liquids tend to display a mesoscopic ordering due to the competition between ionic and van der Waals interactions. Super-concentrated electrolytes on the other hand develop an ordering as a result of local coordination responsible for the solvation of the ions. This can also be expected to influence the dynamic behaviour and hence in the end the ion transport.

In this thesis the structure and dynamics of these systems have been investigated using X-ray and neutron scattering techniques identifying common structural features between ionic liquids and super-concentrated electrolytes as well as multiple relaxation processes at different length scales. Moreover, the first solvation shells and molecular interactions were determined by Raman spectroscopy and the results linked to macroscopic properties, such as the phase behaviour and the ionic conductivity.

**KEYWORDS:** ionic liquid, lithium ion battery, electrolyte, TFSI, imidazolium, pyrrolidinium, organic solvent, Raman scattering, SAXS, NSE.

## List of publications

This thesis is based on the following publications

- I. Solvation of Li<sup>+</sup> and Na<sup>+</sup> in carbonate based battery electrolytes – a combined computational and spectroscopic study  
E. Jonsson, L. Aguilera, D. Monti, A. Matic and P. Johansson  
Submitted
- II. A structural study of LiTFSI-tetraglyme mixtures: From diluted solutions to solvated ionic liquids  
L. Aguilera, S. Xiong, J. Scheers and A. Matic  
Journal of Molecular Liquids **210**, 238-242 (2015)
- III. Structure of super-concentrated LiTFSI in acetonitrile and propylene carbonate electrolytes  
L. Aguilera, J. Scheers and A. Matic  
Manuscript
- IV. Enhanced low-temperature ionic conductivity via different Li<sup>+</sup> solvated clusters in organic solvent/ionic liquid mixed electrolytes  
L. Aguilera, J. Scheers and A. Matic  
Accepted
- V. The effect of lithium salt doping on the nanostructure of ionic liquids  
L. Aguilera, J. Völkner, A. Labrador and A. Matic  
Physical Chemistry Chemical Physics **17**, 27082-27087 (2015)
- VI. Mesoscopic dynamics in lithium salt doped imidazolium based ionic liquids  
L. Aguilera, J. Verwohlt, C. Gutt, A. Faraone, Gunnar Westman and A. Matic  
Manuscript
- VII. Effect of lithium salt on the stability of dispersions of fumed silica in the ionic liquid BMImBF<sub>4</sub>  
J. Nordström, L. Aguilera and A. Matic  
Langmuir **28**, 4080-4085 (2012)

## **Additional publications not included in this thesis**

- VIII. In-situ gelled electrolyte for lithium battery: electrochemical and Raman characterization”  
L. Lombardo, M. A. Navarra, S. Panero, L. Aguilera, A. Matic and J. Hassoun  
Journal of Power Sources **245**, 232-235 (2014).
- IX.  $\gamma$ -Fe<sub>2</sub>O<sub>3</sub> nanoparticles encapsulated in polypyrrole for quasi-solid-state lithium batteries  
J. K. Kim, L. Aguilera, F. Croce and J. H. Ahn  
Journal of Materials Chemistry A **2**, 3551-3556, (2014).
- X. Role of organic solvent addition to ionic liquid electrolytes for lithium-sulphur batteries  
S. Xiong, J. Scheers, L. Aguilera, D. H. Lim, K. Xie, P. Jacobsson and A. Matic  
RSC Advances **5**, 2122-2128 (2015).
- XI. Encapsulation of paclitaxel into a bio-nanocomposite. A study combining inelastic neutron scattering to thermal analysis and infrared spectroscopy  
M. Martins, A. Orecchini, L. Aguilera, J. Ecker, J. Embs, A. Matic, M. Saeki and H. Bordallo  
EPJ Web of conferences **83**, art. No. 02011, (2015).
- XII. Enhanced Ionic Mobility in Nano-porous Silica by Controlled Surface Interactions  
M. Nagendrachar Garaga, L. Aguilera, N. Yaghini, A. Matic, M. Persson and A. Martinelli  
Submitted

## **Contribution report**

### **Paper I**

I performed the Raman measurements, data analysis and wrote the corresponding part. I co-authored the paper with my colleagues.

### **Paper II**

I performed the SAXS experiments and the overall data analysis. I wrote the main part of the article. Simulations were done by JS and Raman by SX.

### **Paper III**

I performed all the experiments and the data analysis. I wrote the main part of the article. Simulations were done by JS.

### **Paper IV**

I performed most of the experiments and the overall data analysis. I wrote the main part of the article. Simulations were done by JS.

### **Paper V**

I performed all the experiments and the data analysis. I wrote the main part of the article.

### **Paper VI**

I performed all the experiments and the data analysis. I wrote the main part of the article.

### **Paper VII**

I proposed the model used to interpret the data, contributed to sample preparation and DSC measurements. I co-authored the paper with my colleagues.

## Table of Contents

---

<b>CHAPTER 1 INTRODUCTION</b>	<b>1</b>
<b>CHAPTER 2 BATTERIES</b>	<b>3</b>
<b>2.1 THE LITHIUM ION BATTERY</b>	<b>4</b>
<b>2.2 ELECTROLYTES</b>	<b>4</b>
2.2.1 ORGANIC SOLVENT BASED ELECTROLYTES	5
2.2.2 SUPER-CONCENTRATED ELECTROLYTES	6
2.2.3 IONIC LIQUID BASED ELECTROLYTES	8
2.2.4 SOLVATED IONIC LIQUIDS	8
2.2.5 MIXED ELECTROLYTES	9
<b>CHAPTER 3 STRUCTURE AND DYNAMICS IN ELECTROLYTE SOLUTIONS</b>	<b>11</b>
<b>3.1 IONIC SOLVATION</b>	<b>11</b>
3.1.1 FROM DILUTE SOLUTIONS TO IONIC LIQUIDS	14
<b>3.2 NANOSTRUCTURE IN ELECTROLYTES</b>	<b>17</b>
3.2.1 CHARGE ALTERNATION	17
3.2.2 POLARITY DOMAINS	19
<b>3.3 DYNAMICS IN ELECTROLYTES</b>	<b>20</b>
<b>CHAPTER 4 EXPERIMENTAL TECHNIQUES</b>	<b>25</b>
<b>4.1 DIFFERENTIAL SCANNING CALORIMETRY</b>	<b>25</b>
<b>4.2 DIELECTRIC SPECTROSCOPY</b>	<b>27</b>
4.2.1 BASIC THEORY	27
<b>4.3 RAMAN SPECTROSCOPY</b>	<b>29</b>
4.3.1 CLASSICAL TREATMENT OF THE RAMAN EFFECT	30
4.3.2 INSTRUMENTAL DETAILS AND DATA TREATMENT	31
<b>4.4 SMALL ANGLE X-RAY SCATTERING</b>	<b>32</b>
4.4.1 BASIC THEORY	32
4.4.2 INSTRUMENTAL DETAILS AND DATA TREATMENT	33
<b>4.5 NEUTRON SPIN ECHO</b>	<b>34</b>
<b>CHAPTER 5 SUMMARY OF APPENDED PAPERS</b>	<b>37</b>
<b>OUTLOOK AND ACKNOWLEDGMENTS</b>	<b>45</b>
<b>BIBLIOGRAPHY</b>	<b>47</b>



# Chapter 1

## Introduction

---

As oil resources continuously decrease and concerns about climate changes keep growing, the call for green energy alternatives, such as solar, tidal, and wind energy, constantly increases. However, wind does not blow to our will and sun does not shine the whole day, so efficient means of energy storage are needed in order to take the best advantage of these intermittent energy sources. Lithium-ion batteries (LIBs) have placed themselves among the strongest candidates to fulfill this task, mainly due to their high-energy efficiency, high specific capacity, and long cycle life [1,2]. Although LIBs are established commercial products, they are currently most suitable for portable applications, such as mobile devices. When it comes to larger applications, such as electro mobility, i.e. the substitution of the internal combustion engine in vehicles, either hybrid (HEVs) or ideally electric vehicles (EV), the demands are stricter. For instance, the energy density needs to be increased as well as the cycle life, yet keeping safety at the highest standard. As a consequence, LIBs have been in the scope of intense research in recent years to improve the performance.

The electrolyte in current state-of-the-art LIBs contains a combination of organic solvents, such as dimethyl carbonate (DMC), propylene carbonate (PC), or ethylene carbonate (EC), and a salt, such as lithium hexafluorophosphate ( $\text{LiPF}_6$ ). However, these electrolyte formulations are highly flammable and already at relatively low temperatures (80 °C) the Li-salt decomposes into hazardous gases [3]. In response to this, vast efforts have been directed to implement new additives to reduce the flammability and prevent decomposition of such electrolytes, yet without hindering the desired high ionic conductivity nor reducing cycling performance [4,5]. However, to truly revolutionize the LIB, new electrolyte concepts need to be implemented.

Recent studies have found that the electrochemical nature of organic solutions drastically change over a certain threshold of Li-salt concentration, i.e. 1-5 solvent molecules per lithium [6-11]. These so-called super-concentrated electrolytes not only allow for fast charging, but also long lasting LIBs [6,12]. Against the conventional believe that optimal electrolytes should have a low viscosity, super-concentrated electrolytes are viscous but provide a very large amount of charge carries, in some cases comparable or even exceeding the carrier density in typical ionic liquids (ILs). Thus, different transport mechanisms are most likely present in these systems.

Ionic liquids are as well attractive materials to be implemented in future battery technologies. Defined as molten salts with melting temperatures below 100 °C, hence composed only of ions, they present interesting properties. On one hand, they possess low vapor pressure and low flammability, which enhance the safety features of an electrolyte. On the other hand, they have an intrinsic high charge carrier density and are capable to dissolve different, and high amounts of, lithium salts. These properties have encouraged the research community to investigate the performance of ILs not only as additives to, or mixtures with, organic solvents, but also as full replacements of current electrolyte solvents [13-16]. Furthermore, some ILs present an atypical structuring at a mesoscopic scale, i.e. 10-20 nm [17-19]. This structuring comes from the segregation of polar and apolar domains [18,20-22].

Given the ionic nature of both ILs and super-concentrated electrolytes it is not naive to believe they could share some properties. Indeed, some super-concentrated solutions can form IL-like electrolytes; “solvated ionic liquids” [9]. Solvated ionic liquids interestingly gather the best of two worlds; the thermal stability and high carrier density from ILs and the electrochemical performance of super-concentrated electrolytes. Although many studies have shown improvement in electrochemical stability window and cycle performance, the origin these features is not clear. Hence, a deeper understanding of the structure and dynamics could provide the basis to the development of better performing LIBs. Despite the promising properties of IL based electrolytes, problems such as increased viscosity, low cycle performance and low rate capability keep them being implemented in LIBs. Whether it is an intrinsic problem of the ILs, a poor choice of the components, or even the use of the wrong concentration range, it is a topic worth to investigate.

This thesis focuses on the structural and dynamical features of different ILs and super-concentrated electrolytes at different length scales. The solvation shell and local coordination has been studied by Raman spectroscopy, whereas the mesoscopic structure has been studied by means of neutron and X-ray scattering techniques. Moreover, the dynamics associated at mesoscopic length scales has been studied by means of neutron scattering experiments. The findings of the local structures and dynamics are correlated with macroscopic properties such as ionic conductivity and phase behavior studied by dielectric spectroscopy and differential scanning calorimetry, respectively.

# Chapter 2

## Batteries

---

A battery is a device that converts chemical energy stored in a material directly into electric energy by means of an electrochemical reduction-oxidation (redox) reaction [23]. Although the term “battery” is commonly used, the proper name of the basic electrochemical unit is the “cell”. Hence, a battery consist of one or more electrochemical cells which are connected in series or in parallel in order to achieve the desired current, or voltage, for a given application.

The three major components that form a cell are:

*Anode:* This is the negative electrode that gives up electrons and is oxidized during an electrochemical reaction during discharge.

*Cathode:* This is the positive electrode that accepts electrons from the external circuit and is reduced during the electrochemical reaction during discharge.

*Electrolyte:* This is the medium that allows the transfer of ions between anode and cathode.

Batteries can be classified as primary and secondary. Primary batteries can only be used one time (nonrechargeable), whereas secondary batteries can be used multiple times (rechargeable). In a rechargeable system, the battery is charged by reversing the natural discharge process by means of an external driving force. During the charge process the roles of the electrodes are exchanged.

One of the major challenges when building a battery is to find the right combination of materials to provide a high energy density, high specific capacity, and long term cycleability, yet keeping the cost as low as possible, maintaining certain degree of safety, and producing it in a sustainable way.

## 2.1 The lithium ion battery

Among the large variety of secondary batteries, the one that has come on top is the lithium-ion battery. In this system, the cathode is usually a metal oxide, and the anode is typically graphite [24]. In Figure 1 the schematic drawing of a LIB and its components is presented. The charge and discharge processes result from the insertion and extraction of the lithium ions from the interstitial spaces between the atomic layers of the electrodes. LIBs possess both, high energy density (~200 Wh/Kg) and specific density (~250 Wh/L) [25], which makes them attractive for applications where weight and volume are critical. However, current technology is only suitable for portable devices. When implemented into larger applications, such as hybrid electric vehicles or electric vehicles, safety becomes utterly important.

State-of-the-art LIBs generally contain an organic solvent-based electrolyte, which inherently has a high vapor pressure, and a high flammability. Moreover, the salts commonly used are fluorine based, hence upon decomposition there is a risk that hazardous hydrofluoric acid is produced [3,26]. Therefore the search of new electrolyte formulations, which are not only intrinsically safer, but also provide a larger electrochemical window, and higher rate capability, will enable the EV market to finally take its deserved position in society.

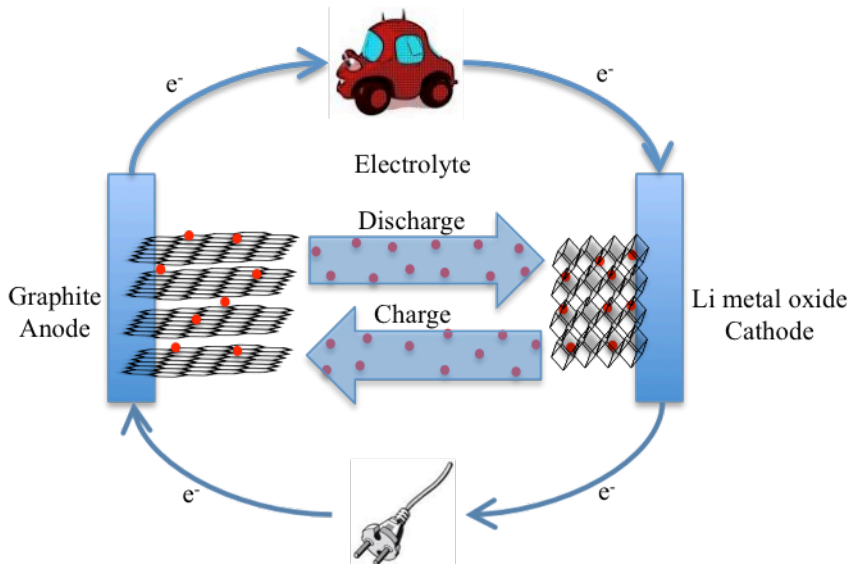


Figure 1. Basic components of a lithium-ion battery and the charge-discharge processes.

## 2.2 Electrolytes

An electrolyte is a medium that conducts ions. The role of the electrolyte in a battery is to transport ions from one electrode to another; hence, one of the primary requirements of a good electrolyte is to provide fast and efficient ion transport, which is usually referred to as the ionic conductivity. However, this is not the only

requirement that the electrolyte must fulfill. In general a good electrolyte should comply with the following requirements [27]:

- a) To be a good ionic conductor ( $\sigma \geq 10^{-3} \text{ Scm}^{-1}$ ) and electronic insulator, this is to facilitate the transport of ions without allowing self-discharge of the cell.
- b) To have a wide electrochemical stability window (ESW) (often ca. 0-5 V vs  $\text{Li}^+|\text{Li}$ ) so that it does not decompose at the working potentials of the electrodes.
- c) It should be inert with respect to the other cell components.
- d) It should be able to withstand electrical, mechanical or thermal abuses.
- e) It should be environmental friendly and relatively inexpensive.

Although the perfect electrolyte should comply with all of these properties, most of the time only a compromise can be found. With the advent of new battery systems new complications arise, e.g. small variations in the cell chemistry could result in drastic changes in the choice of electrolyte. For this reason, a thorough characterization of the electrolyte not only from an electrochemical, but also from a structural and dynamic point of view is necessary.

Many electrolyte concepts have recently been introduced. They range from the commonly used organic solvent electrolytes where small amount of additives are implemented, to more innovative approaches where the salts concentration are taken to their limits or even drastic changes such as the use of ionic liquids as solvents. Each of them has its advantages and disadvantages and will be further discussed during this Chapter.

### ***2.2.1 Organic solvent based electrolytes***

When using organic solvents as the base for an electrolyte one of the prime properties is the dielectric constant, basically the higher the better. This allows the dissolution of a large variety of salts in a broad concentration range. Cyclic carbonates are among the most common solvents. In fact, the first commercially available LIB used propylene carbonate (PC) as a solvent in combination with an amorphous carbon anode [28]. PC not only possesses a high dielectric constant ( $\epsilon \approx 64$  at 25 °C) [29], but also remains liquid over a broad range of temperatures. However, it is not suitable when graphite is used as an anode, due to the continuous decomposition of the electrolyte and the exfoliation of the anode [30].

A cousin of PC, ethylene carbonate (EC), has an even higher dielectric constant ( $\epsilon \approx 90$  at 35 °C) [29]. However, EC creates a passivation layer on the interface between the electrolyte and the anode [31], which prevents the decomposition of the electrolyte, hence a good cycling performance is obtained. Nevertheless, the high melting point of EC makes it unsuitable for room temperature applications. Thus, other solvents are added to decrease the melting point, e.g. the mixture of EC and PC, with  $\text{LiPF}_6$  as the salt, as proposed by Fong et al. [30]. This mixture provides good cycling performance, wide working temperature range, and sufficient ionic conductivity. A similar mixture was patented by Sony and introduced into a commercial LIB in 1990 [32].

To the date, no single solvent can meet all the requirements for a “perfect” electrolyte; therefore, a mixture of several of them is used in practice, as shown by the example above. For instance, linear carbonates such as dimethyl carbonate (DMC) or diethyl carbonate (DEC) are usually mixed with cyclic carbonates to decrease the viscosity and lower the melting point. Following this approach, Tarascon et al. have tested several mixtures of organic solvents and lithium salts in order to determine the most suitable electrolyte [33]. A compromise between ionic conductivity, electrochemical stability window, and liquid range was used to determine that the best electrolyte was a combination of EC and DMC as solvent and ca. 1 molar concentration of fluorinated lithium salt.

To the date, state-of-the-art batteries include a mixture of organic solvents, usually EC and DMC, each of them added to fulfill a specific task, and a dissolved salt, such as LiPF<sub>6</sub>, typical with a concentration of 1 molar. Although, it has been demonstrated that LiPF<sub>6</sub> is thermally unstable and decomposes into hazardous gases [34,35], and that the organic solvents are generally flammable and volatile [36-38], these kind of electrolytes are still the best compromise between performance and safety, hence they are present in the vast majority of available LIBs on the market. In Figure 2 some of the most common organic solvents and lithium salts are presented.

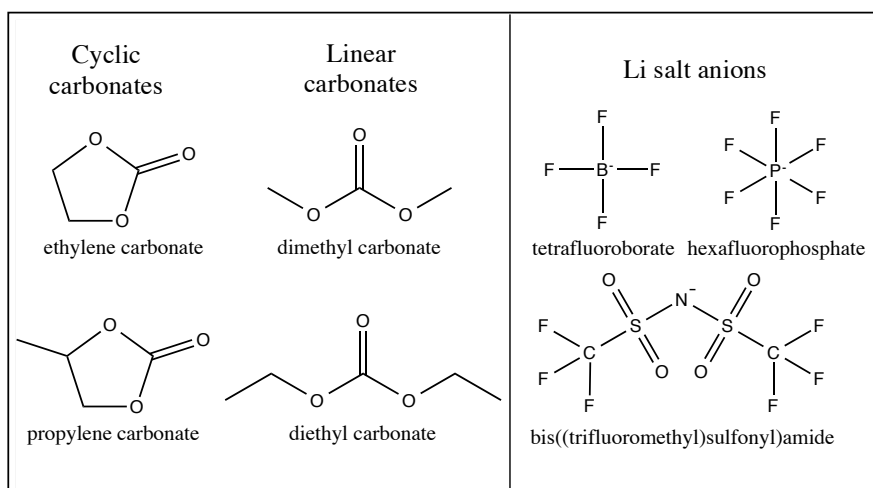


Figure 2. Common organic solvents and lithium salts used in lithium-ion batteries.

### 2.2.2 Super-concentrated electrolytes

Super-concentrated (or highly concentrated) electrolytes have recently received considerable attention in battery applications [6,10-12,39-41]. The term super-concentrated is given to electrolyte solutions with salt concentrations typically ranging between 1 to 5 solvent molecules per lithium ion (ca. 3 to 5 molar), much higher than in standard electrolytes. A peculiarity of super-concentrated electrolytes is that most of the solvent molecules are directly interacting with the ions; hence the bulk properties of the neat solvent are lost. To clarify the concept in Figure 3 a schematic picture of a standard electrolyte as well as a super-concentrated electrolyte are shown.

Generally the addition of Li-salt to a solvent increases the ionic conductivity due to the increased amount of charge carries, however this is only valid to a certain extent. When the Li-salt concentration exceeds a certain threshold, the coulombic interactions in the electrolyte increase and the viscosity becomes so high that the large number of carries do not compensate for the slow down of the dynamics, i.e. the ionic conductivity decreases [42]. This is unfavorable for a LIB and results in poor rate performance. However, recent discoveries have stimulated intensive research activities on super-concentrated electrolytes for LIBs. For instance, solvents that before were excluded due to detrimental effects such as decomposition at the electrode-electrolyte interphase or low ESW have recently shown to drastically change their electrochemical properties when used at high salt concentrations [6,10-12]. For example, super-concentrated electrolytes based on PC present a very particular behavior; at low salt concentration PC continuously decomposes at the solvent-electrode interface as well as exfoliates the graphite anode, due to the incapability to form a stable passivation film [30,43]. However, at high concentration of  $\text{LiPF}_6$ , the electrolyte forms a stable passivation film at the anode, allowing for a better cycle performance [44]. A similar behavior has also been reported for other solvents, e.g. acetonitrile. At low salt concentrations acetonitrile will react with lithium, making it an unsuitable candidate to be implemented into LIBs [45]. However, if the concentration of Li-salt is high enough, acetonitrile coordinated to the  $\text{Li}^+$  remains stable towards lithium and good cycle performance is obtained [12]. Besides the improvement in ESW, super-concentrate electrolytes also present interesting properties in their transport behavior. For instance, despite the high viscosity of super-concentrated electrolytes, recent studied have found that fast charge-discharge can be achieved [6]. This result points out that high viscosity might not be a limiting factor for rate performance. In general when the concentration of the salt reaches certain threshold, the vapor pressure of the electrolytes is considerably reduced, as well as its flammability [9,39,40,46]. Thus, the safety is improved.

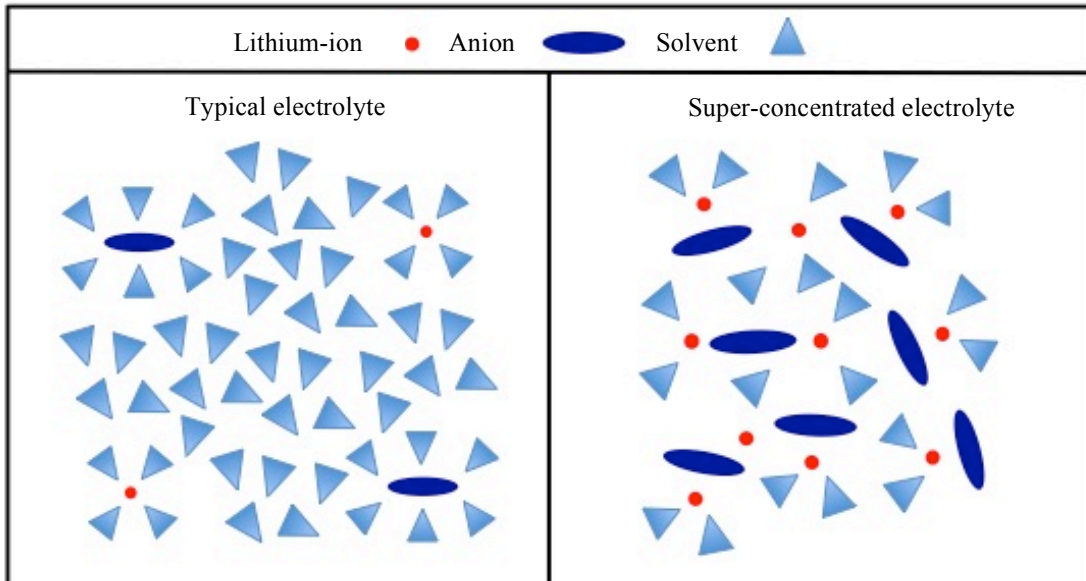


Figure 3. Schematic of standard LIB electrolyte and a super-concentrated electrolyte.

### 2.2.3 Ionic liquid based electrolytes

Ionic liquids are liquids that consist exclusively of ions, hence they are extremely attractive as electrolytes. This definition includes liquids that are known as molten salts, which usually have higher melting temperatures. However, in the last decades the term “ionic liquids” has been limited to those molten salts which have melting points below 100 °C [47]. Among the general properties of ILs, it is worth to mention the high thermal stability [48,49], low vapor pressure [49,50], non-flammability [51], wide ESW [52], and high ionic conductivity [53,54]. With these characteristics, it is easy to realize why the research community has put such a strong focus in the study of these systems. ILs are today found in a range of different applications, e.g. as electroplating solvents [55,56], catalysts [57,58], and of course as electrolytes [16,59]. In the particular case of ILs as the basis for electrolytes, applications have been proven at laboratory scale for solar cells [60], fuel cells [61], and LIBs [62,63].

The usual approach taken in order to use ILs as electrolytes for LIBs, is to include a lithium salt which shares the same anion as the IL [64,65]. ILs can be synthesized with the typical anions used in the battery field such as  $\text{PF}_6^-$ , TFSI, and  $\text{CF}_3\text{SO}_3^-$ . Large amounts of salt can usually be dissolved, making the concentration comparable to super-concentrated electrolytes. However, upon the addition of the lithium salt to the IL, the viscosity increases relatively fast [64].

Among the large variety of ILs, those containing bis(trifluoromethylsulfonyl)-imide, TFSI, have been highlighted as strong candidates to be implemented into LIBs. Due to the TFSI anion’s charge delocalization and flexible nature [66], TFSI based-ILs are usually liquid at room temperature. In addition, they present a wide ESW [52] and a lower viscosity than ILs sharing the same cation but with smaller anions [67]. One of the most widely used cations in LIBs are those belonging to the pyrrolidinium family, mainly due to the large ESW when used with TFSI (-0.5 to 5.5 V vs  $\text{Li}^+/\text{Li}$ ). In Figure 4 two of the most widely used families of cations in IL based electrolytes are presented.

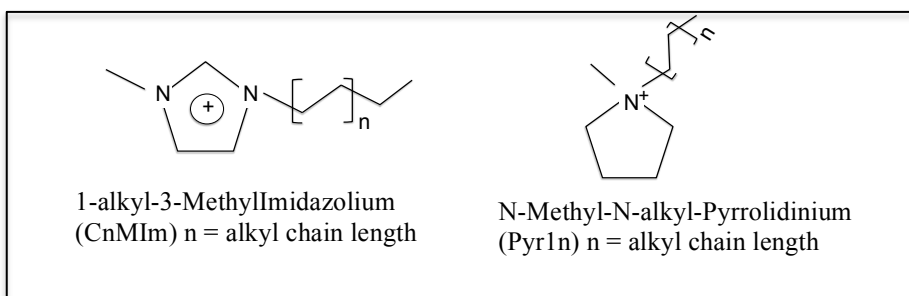


Figure 4. Commonly used cations in LIBs based on, imidazolium and pyrrolidinium.

### 2.2.4 Solvated ionic liquids

Solvated ionic liquids have recently emerged as an alternative to traditional ILs as electrolytes for LIBs. The concept is based on the formation of a complex between an ion and a solvent molecule effectively forming a large ionic species. This concept was

first described by Angell in 1965, when he regarded solvated calcium ions as independent cationic species [68], but it was only recently these systems were named solvated ionic liquids [69].

When implemented in LIBs, a solvated IL that contains  $\text{Li}^+$  can be realized by dissolving the right amount of a Li-salt in a solvent. Prime examples are the equimolar mixtures of triglyme ( $\text{CH}_3\text{O}-(\text{CH}_2\text{O})_3-\text{CH}_3$  (G3)) or tetraglyme ( $\text{CH}_3\text{O}-(\text{CH}_2\text{O})_4-\text{CH}_3$  (G4)) and a Li-salt, e.g. LiTFSI [41,46,70], as shown in Figure 5. In these particular cases the ratio of solvent oxygens to  $\text{Li}^+$   $[\text{O}]/[\text{Li}^+]$  is 4-5, which means that each  $\text{Li}^+$ , in theory, could be precisely solvated by a single solvent molecule. These solvated ILs share most of the advantageous properties of the ILs, but with the difference that Li-ions already are present.

Although solvated ILs are generally more viscous than the standard electrolytes, work performed by Yoshida et al. suggested that the transport mechanism associated with the  $\text{Li}^+$  might be migration from one site to another and not diffusive, which could result in improved transport properties [71], including increased  $\text{Li}^+$  transference numbers [70]. In general, just like the highly concentrated electrolytes, solvated ionic liquids have typically low vapor pressure and increased ESW [9,71].

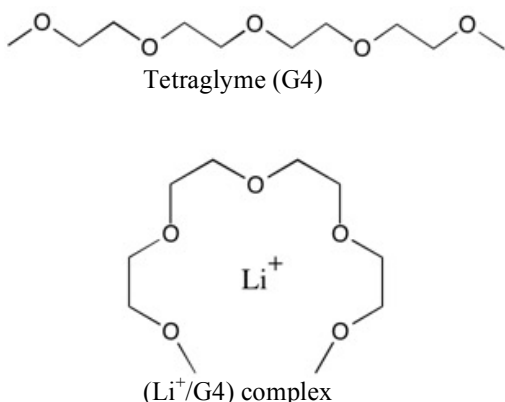


Figure 5. Schematic representation of the structure of a tetraglyme molecule (top) and a  $\text{Li}^+$ /G4 complex (bottom).

### 2.2.5 Mixed electrolytes

An intermediate stage between fully replacing the traditional organic solvents, i.e. introducing a completely new electrolyte, is the partial replacement of one or more of the components. In this chapter, the advantages and drawbacks of organic solvents and ionic liquid based electrolytes respectively, have been discussed. However, a possible approach to overcome the problems that arise from the intrinsic properties of the respective materials is to use combinations or hybrids.

In many cases, the addition of ILs to organic solvent-based electrolytes can effectively reduce the flammability [15,36,51,72-74]. Furthermore, some ILs have shown to be capable of dissolving high amounts of carbon dioxide (CO<sub>2</sub>) [75]. CO<sub>2</sub> is generated at the cell level as a result of electrolyte decomposition at the electrode interface [76-78]. Although the amount of gas generated is usually low, with time the

cell can build up pressure, which eventually could result in failures at the cell level or, in the worst case, explosions. Favorable results have been obtained, however there is still a lack of understanding on how the addition of ILs affects the overall properties of the system and therefore further research need to be done.

Following a similar approach, the addition of organic solvents to the IL based electrolytes also show encouraging results [14,79,80]. For example, the diffusion coefficient of  $\text{Li}^+$  is considerable increased when choosing organic solvents that preferentially solvate lithium [80]. Moreover, the film forming properties of the organic solvents seem to favor the interfacial reactions at the electrodes [79]. Even though improvements are undeniable, there is still a lack of knowledge on how the solvation shell is actually structured and how it affects the overall properties of the electrolyte.

# Chapter 3

## **Structure and dynamics in electrolyte solutions**

---

The electrolyte concepts described in Chapter 2 are all liquids. As in all liquids the molecular arrangement and the nature of the interactions in the electrolyte will determine the macroscopic properties of the system. While the local structure around the  $\text{Li}^+$  will be closely related to the transport properties of the electrolyte, the strength of the interactions can also influence properties such as the ESW or the reaction rate at the electrodes. Moreover, the presence of mesoscopic heterogeneities can also influence the diffusivity of  $\text{Li}^+$  and give raise to collective motions that might influence the overall performance in LIBs. Hence, the study of the structure and the dynamic behavior in liquid electrolytes is of importance. In this Chapter the structural and dynamical aspects of the electrolytes at different length scales are discussed and linked to macroscopic properties.

### **3.1 Ionic solvation**

According to the definition provided by the IUPAC, solvation is any stabilizing interaction of a solute and a solvent [81]. In our particular case the solute is a Li-salt. As the salt dissociates the ions spread out and become surrounded by the solvent molecules upon reaching equilibrium. However, a term that is perhaps more familiar and relevant is the solvation shell. In general for electrolyte solutions, the solvation shell is defined as the molecules that surround the ions, hence, behave different from the bulk solvent molecules, see Figure 6.

Several layers of molecules might form the solvation shell, those molecules found on the first solvation shell are usually said to be “coordinated” to the ions. It is common in literature to find coordination numbers reported, however, it is important to clarify that the coordination number is not directly related to the number of molecules in the first solvation shell, this is the solvation number, but to the number of atoms directly linked to the ion. Much information can be found in literature regarding the average solvation numbers. However, studies that describe the actual composition of the solvation shell are more scarce [82]. Hence, in the appended papers number I and IV a contribution in this direction is presented, by proposing models that represents how the actual solvation shell in multicomponent electrolytes might be composed as well as to what extent these kinds of configurations contribute to the average solvation numbers.

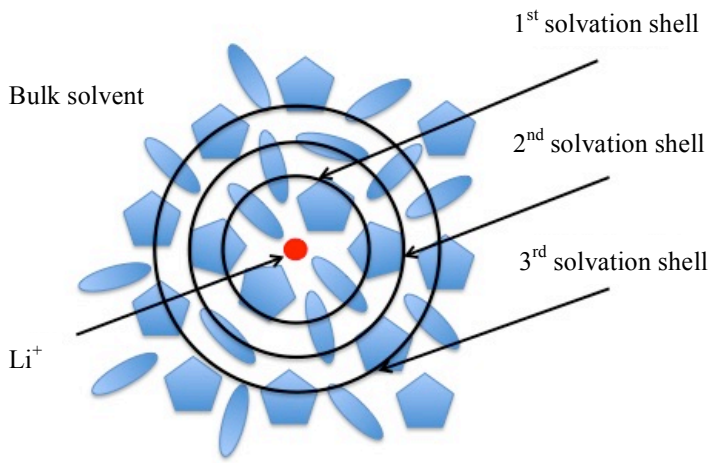


Figure 6. Schematic of a typical solvation shell in a mixed solution, where the  $\text{Li}^+$  is fully solvated.

In Figure 6 the ideal scenario for a completely solvated  $\text{Li}^+$  is shown, however, this is not always the case. For instance, if the solubility of the salt is limited or if the salt concentration is too high, the salt might not be fully dissociated or the solvation shells might come in close contact with each other. In literature it is common to find terms such as solvent separated ion pairs (SSIP), contact ion pairs (CIP) and aggregates, see Figure 7. SSIP refers to those ions that are separated from each other by about a single solvent molecule. CIP are configurations where the anion and cation are in direct contact with each other, as in the case when the anion is part of the solvation shell. Finally, aggregates are those where more than two ions are in direct contact or coordinated to each other.

The actual configuration of the solvation shell is of great relevance and dictates many of the properties of the electrolyte. For example, configuration where ions are paired could effectively reduce the ionic conductivity. Ion pairs could have a neutral net charge and therefore do not contribute to ion conduction. Furthermore, if the coordination shell is strongly interacting with the  $\text{Li}^+$ , the probability of the  $\text{Li}^+$  to react upon reaching one of the electrodes is reduced. This effect usually causes a decrease in the rate capability. Additionally, the interaction between the  $\text{Li}^+$  and the coordinated molecules can in some cases change the electrochemical stability of the electrolyte compared to the neat solution resulting in an improvement in battery performance. These are a few examples of the role of the solvation shell in electrolytes and will be discussed further in the following sections.

There are many experimental techniques that can be used to study the composition of the solvation shell. For instance, infrared and Raman spectroscopy exploit the high sensitivity of the vibrational modes to the local environment of the molecules to determine the solvation shell in electrolytes. Thus, molecules that are coordinated to an ion will usually show changes in their vibrational frequencies. These changes can be tracked both qualitatively and quantitatively, yielding valuable information on the studied system. As previously mentioned the arrangement of the molecules in a liquid is constantly changing and so is the solvation shell, hence it is important that the

process measured by the instrument is faster than the exchange of the molecules in the solvation shell, which is typical around  $10^{-12}$  to  $10^{-9}$  s depending on the coordination strength. This is a clear advantage of vibrational spectroscopy over other methods since the molecular vibrations are faster ( $10^{-14}$  to  $10^{-12}$  s) than the exchange rate of the molecules in the solvation shell. Hence we can clearly differentiate coordinated from free molecules. Moreover, the selectivity of the vibrational modes allows for the identification of specific configurations. Thus, by simply calculating the area of the respective vibrational modes and knowing the salt concentration in the system and the scattering cross section of the molecules, we can obtain the solvation numbers even in mixed electrolyte systems [83].

Accurate solvation numbers can also be determined by nuclear magnetic resonance (NMR) spectroscopy. When a molecule is coordinated to an ion the chemical shift will be different from that of a free molecule. However, this method requires that the environment remains unchanged for a considerable amount of time i.e.  $10^{-4}$  s. This time is usually much larger than the exchange rate between coordinating and free molecules; hence an average signal would be obtained from the NMR accounting for both. However, there are ways to circumvent this problem, one option is to cool down the system to a point where the dynamics are slow enough to obtain different signals from coordinated and free molecules [84]. Moreover, for many multivalent ions the exchange rate is slow enough to be measured by NMR spectroscopy, which unfortunately is not the case for the  $\text{Li}^+$ . Another option is to estimate the fractions contributing to the average signal, i.e. the pure solvent is measured and together with the signal from the actual electrolyte it is possible to interpolate the chemical shift that one would expect from a system where all the molecules are coordinated, hence obtained the partial contribution of both free and coordinated molecules to the actual measured peak in the electrolyte [85,86].

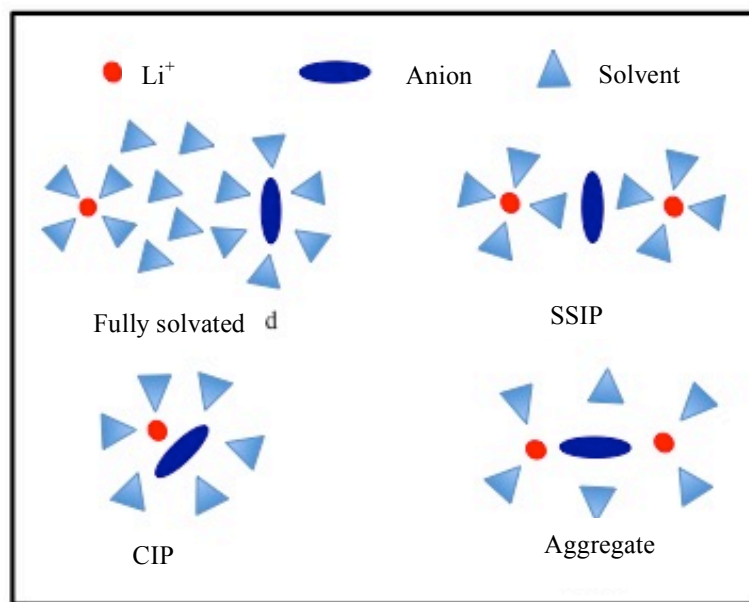


Figure 7. Different solvation scenarios, from fully dissociated salts to aggregates.

### **3.1.1 From dilute solutions to ionic liquids**

In a dilute solution it is assumed that the number of ions is low compared to the number of solvent molecules, hence, a complete dissociation of  $\text{Li}^+$  and anion can be expected. In contrast to this picture, early work by Hyodo and Okabayashi on a lithium  $\text{LiClO}_4/\text{EC}$  electrolyte, demonstrated that already at concentrations around 0.6 molar (M) contact ion pairs are present [87]. This is remarkable since EC possesses one of the highest dielectric constants among the organic solvents, and therefore ion paring would not be expected to occur. In general, the coordination number of  $\text{Li}^+$  is ca. 4 [87-90], however, the actual configuration and components of the solvation shell depends on many factors, such as, solvent salt, concentration and temperature.

In the electrolytes currently used in commercial Li-ion batteries the salt concentration is around 1 M and contains a mixture of organic solvents, such as EC and DMC, and  $\text{LiPF}_6$  as a salt. Here the solvation shell can be composed of a combination of the different organic solvent molecules. In work performed by Borodin and Smith, by means of molecular dynamics simulations, it was found that the probability of having DMC or EC in the first solvation shell was rather equal, in contrast to what one would expect given the large difference in dielectric constants [90]. Moreover, it was also found that the fraction of contact ion pairs increases with the amount of DMC in the electrolyte [90,91]. This example, points out the importance of knowing the components of the solvation shell. Usually, DMC is added in the electrolyte in order to decrease the viscosity of the system, i.e. increase the ionic conductivity. However, if the DMC concentration is too large the number of contact ion pairs would be increased and thus lower the overall  $\text{Li}^+$  transport. Although the ionic conductivity measurement would lead us to the right combination of solvent and salt concentration, as in the work performed by Tarascon et al. [33], it does not provide a deep understanding of the system as when combined with the knowledge acquired from the microscopic structure of the solvation shell.

Both of the previously mentioned studies [33,90] made use of pseudo spherical anions ( $\text{ClO}_4^-$  and  $\text{PF}_6^-$ ), however, it is interesting to consider the effect of introducing a more flexible and asymmetric anion, such as TFSI which is shown in Figure 8. TFSI has a lower symmetry and the ability to change between different conformations. In Figure 8 the two stable conformations, cisoid ( $C_1$ ) and transoid ( $C_2$ ), identified by Raman spectroscopy and supported by computational structures [66,92-96] are illustrated. The energy difference between them is only a few kilojoules indicating that they generally coexist at room temperature [66,96].

Recent work has demonstrated that also when TFSI is used the concentration of CIPs is comparable to electrolytes with  $\text{ClO}_4^-$  and  $\text{PF}_6^-$  salts [97]. Although this result might be misleading by pointing towards a weak effect of the anion, there are other factors to be considered. For instance, the presence of an anion in the first solvation shell does not necessarily imply that the CIP has an effective neutral charge. If the anion is weakly interacting with the  $\text{Li}^+$ , they are still regarded as separated charges, hence contribute to the ionic conductivity [9].



Figure 8. Calculated structures of TFSI conformers. Cisoid ( $C_1$ ) and transoid ( $C_2$ ).

Increasing the Li-salt concentration in an electrolyte could be beneficial for the conductivity by the increase in charge carriers, i.e. increase of  $\text{Li}^+$ . However, as discussed above one can expect that this would lead to an increase in the number of contact ion pairs as well as an increase in viscosity, two factors that both will be detrimental for the ionic conductivity. Despite of these facts different groups have investigated electrolytes at increased salt concentrations obtaining very favorable results, both in the electrochemical performance as well as in the rate capabilities of the batteries as discussed in chapter 2 [6,10,40].

As the concentration of salt is increased, contact ion pairs are more and more common, until reaching a point where aggregates are the dominant species in the electrolyte [12]. As a result of this many new considerations must be taken into account. For instance, as the salt concentration is increased both density and viscosity will increase in most of the electrolytes [42], which consequently reduces the ionic conductivity. Furthermore, in many cases depending on the symmetry of the salt and the solvent, as well as other factors, the melting point of the electrolyte can increase so much that it crystallizes at room temperature, e.g.  $\text{LiPF}_6$  or  $\text{LiTFSI}$  dissolved in acetonitrile. In the former case both the solvent and anion are very symmetric resulting in crystallization of the electrolyte already at low salt concentrations, whereas the latter remains liquid even at fractions of 2 solvent molecules per  $\text{Li}^+$  [98]. However, if propylene carbonate (PC) is used as solvent, high concentrations of both  $\text{LiPF}_6$  and  $\text{LiTFSI}$  can be achieved and a stable solutions obtained at room temperature [11]. The reason for this might be the asymmetric nature of PC, although other effects could also play a role.

In super-concentrated electrolytes, most of the solvent molecules are directly interacting with the  $\text{Li}^+$ . The implications of this can be better understood with an example. For instance, while PC is an unstable solvent at dilute concentrations when a graphite anode is present, its super-concentrated version has a remarkable improvement [44]. At low  $\text{LiPF}_6$  concentration the electrochemical stability of the free PC molecules is lower than of the  $\text{PF}_6^-$ , therefore there is a continuous decomposition of PC at the anode interphase, which leads to cell failure. However, when most of the PC molecules are coordinated to the  $\text{Li}^+$ , the electrochemical stability of PC becomes higher or at least comparable to the  $\text{PF}_6^-$ , thus a stable passivation film is deposited on the anode as a result of  $\text{PF}_6^-$  decomposition. Similar examples can be found in literature where a change in electrochemical stability due to the high Li-salt concentration results in improved battery performance [12,99]. In general, super-concentrated electrolytes have low flammability as well a low vapor pressure, which is a result from having almost no free solvent molecules on the system [9,39].

In solvated ionic liquids the concentration of Li-salt is comparable to that of super-concentrated electrolytes, thus most of the solvent molecules are also directly interacting with  $\text{Li}^+$ . Prime examples of solvated ILs are the equimolar mixtures of triglyme or tetraglyme with LiTFSI [9]. The fundamental difference that makes solvated ILs so special is the ability of the solvent molecules to make stable complexes with the  $\text{Li}^+$  and the high ionicity of the electrolyte. To achieve this, the choice of Li-salt is very important. If the anion interacts strongly with  $\text{Li}^+$ , the electrolytes will have a low ionicity and a high fraction of contact ion pairs. However, if the anion weakly interacts with the  $\text{Li}^+$ , as in the case of TFSI<sup>-</sup>, the ionicity of the system will be much higher, and a stable complex between the glyme and  $\text{Li}^+$  will be formed [9]. Therefore, in solvated ionic liquids  $\text{Li}^+$  preferentially coordinates to the glyme and forms a stable complex with a life-time comparable to the diffusive motion. Moreover, in super-concentrated electrolytes there is a high fraction of aggregates and contact ion pairs, in contrast to the lower fraction of contact ion pairs found in solvated ionic liquids.

An ultimate system exploiting the benefits of high  $\text{Li}^+$  concentrations would be a lithium salt that is liquid at room temperature, i.e. a lithium-based ionic liquid. In this way, half of the charge carries would be  $\text{Li}^+$ . However, due to the localized charge of the  $\text{Li}^+$ , its small size, and its symmetry, it is difficult to realize a lithium-based room temperature IL [100]. An alternative to have an IL with  $\text{Li}^+$  as cation is to use an IL with a larger cationic species that allows for the system to be liquid below room temperature, and dope it with a large amount of Li-salt. However, as one would expect, the  $\text{Li}^+$  is usually coordinated by a few anions forming aggregates [64]. Due to the strong ionic nature of the  $\text{Li}^+$ , the interaction with the anion is relatively strong, effectively resulting in large aggregates, thus decreasing the mobility of the  $\text{Li}^+$ . Moreover, the stability of such aggregates reduces the reaction rate of the  $\text{Li}^+$  at the electrode-electrolyte interface which results in low rate capability [79]. Furthermore, the combined effect of large aggregates and strong ionic integrations usually results in drastic increases in viscosity as the concentration of Li-salt is increased [101-103].

An approach to overcome the low diffusivity of the  $\text{Li}^+$  in ILs, mixtures of organic solvents and ILs has been proposed to not only improve the transport properties, but also the electrochemical and thermal stability of the electrolytes [15,73,79,80,104]. The addition of ILs to organic solvents, for example, suppresses the flammability considerably, provided that the IL concentration is high enough [36,74,104]. The reduced flammability comes as a result of the interaction between the organic solvent and the ions. In the pure organic solvent electrolyte the solvent molecules are in excess and therefore are free to be ignited. However, when an IL is used as an additive, the salt concentration is effectively increased, resulting in a situation where most of the solvent molecules coordinate to the ions. If the scenario is turned around and the organic solvent is added to the IL based electrolyte, the organic solvent molecules will preferentially participate in the solvation of  $\text{Li}^+$  [105]. A solvation shell composed by organic solvent molecules screens the charge of the  $\text{Li}^+$ , thus reducing the coulombic interactions with the medium. Hence, with as low as 20 % of organic solvent in the IL electrolyte the diffusivity of the  $\text{Li}^+$  can be doubled [80].

Through the examples in this section it has been demonstrated that changes in the solvation shell have strong implications on the overall performance of the electrolyte. Therefore several of the publications included in this thesis have a strong focus on

determining the solvating structures and how they correlate with the macroscopic properties of the electrolytes.

### **3.2 Nanostructure in electrolytes**

Typically when we think about liquids we think about a disordered medium and indeed most liquids will only have short-range order, i.e. order in the first solvation shell. In an X-ray diffraction experiment this is typical represented with a large and broad single peak in the static structure factor,  $S(Q)$ , between 1-2 Å<sup>-1</sup>, see Figure 9. In this peak intra and inter molecular correlations from neighboring atoms are the main contributions.

In an electrolyte the presence of Li<sup>+</sup> will induce changes in this local structures as discussed in the previous sections. Additionally, through the formation of aggregates ordering at longer length scales can also be induced. In the particular case of ionic liquids the competition between coulombic and van der Waals interactions can lead to the structuring of the liquid on remarkably long length scales. In this chapter this ordering in liquid electrolytes beyond the first solvation shell is discussed.

#### **3.2.1 Charge alternation**

In most of the liquids a short-range order that only expands to the closest neighbors is present. However, in the particular case of ILs the fact that there are only ions in the liquid new considerations must be taken into account. To preserve charge neutrality there has to be charge alternation, i.e. an anion must be neighbor to a cation and vice versa. One of the first studies to report this behavior in ILs was performed by Hardacre et al. on 1,3-dimethylimidazolium chloride (DMIM-Cl) [106]. By means of neutron diffraction it was found that a distance associated with charge ordering was present, and that it resembled that of the crystalline state, however only expanding 5 to 10 Å. It is reasonable to assume that features related to the charge alternation will scale with the size of the ions, and indeed this has been demonstrated by systematically increasing the size of the anions [107]. This finding has also been corroborated by simulations [21,22,108].

In Figure 9 a schematic of different models in which the ions of an IL can order is presented as well as their respective contributions to the static structure factor,  $S(Q)$ . From the models presented in Figure 9 perhaps it is more correct to say that the size of the charge alternation domains (b in the figure) are related to the charged part of the ion and not its total size. An interesting question is the implications of introducing a Li-salt into the system. As previously mentioned the presence of Li<sup>+</sup> in IL based electrolytes causes the formation of large aggregates. The formation of aggregates is directly related to the interaction of neighboring ions, thus, changes in the charge alternation domains are expected [18]. The introduction of a smaller ion such as Li<sup>+</sup>, would in theory make the charge correlation shorter, however, if we consider that the formed aggregate has an effective negative charge and is large in size, it would result in a longer correlation length, which is indeed observed experimentally[18].

Charge alternation ordering is not necessarily an exclusive feature of ILs. In some cases, when the salt concentration is relatively high, we can expect some sort of ionic

ordering, see Figure 10. An example of this phenomenon can be observed in solvated ILs [9]. Here, the tetraglyme solvating the  $\text{Li}^+$ , acting as a cationic species, and the TFSI anion are the only two species present and both have a net charge, hence charge alternation can also be expected in this system. Indeed, the presence of charge alternation domains have been reported in the appended paper II of this thesis [109]. The static structure factor clearly shows a contribution from the charge alternation, the position of the peak in  $S(Q)$  coincides with the distance related to the center of mass of the TFSI to the solvated  $\text{Li}^+$ . This finding has also later been confirmed by Ueno et al. [110].

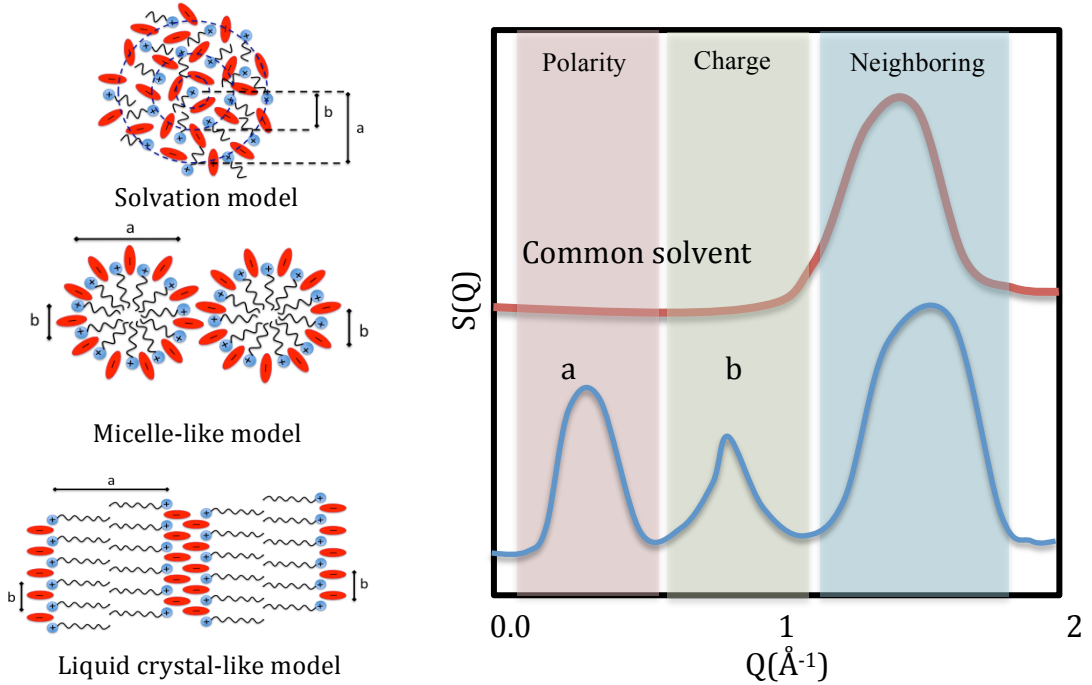


Figure 9. Left: schematic representations of different models to interpret the origin of the peaks found in a typical  $S(Q)$  of an IL. Right: an schematic of a typical  $S(Q)$  from an IL where the contribution of polar, charge alternation and neighboring domains are presented.

Charge alternation domains are present also in super-concentrated electrolytes, see Figure 10. As the salt concentration is increased, the probability of finding an anion in the first solvation shell of  $\text{Li}^+$  is increased. Hence in a certain concentration range, a well-defined charge ordering will start to appear. The concentration range may differ depending on the solvent used or/and the anion, but in general this feature will appear when the solvation shells of the  $\text{Li}^+$  start to be in contact with each other, i.e. there are no free solvent molecules, as shown in the paper III of this thesis.

IL

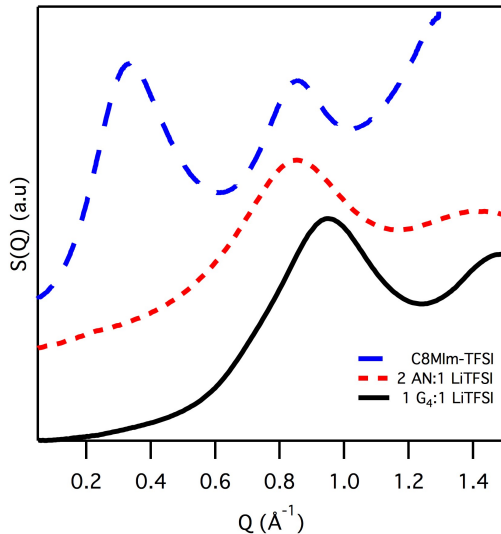


Figure 10. Static structure factor  $S(Q)$  of the solvated IL G4:LiTFSI, the super-concentrated electrolyte 2 AN:1 LiTFSI and the IL C8MIm-TFSI.

### 3.2.2 Polarity domains

The self-aggregation of molecules is a widely studied topic in biology and pharmaceutics. It usually involves the combination of different molecules that will self-assemble as a result of repulsive and attractive interaction between them. A similar behavior has also been observed in ILs [19,20,111]. This is closely related to the introduction of large alkyl groups resulting in the occurrence of structural heterogeneities on mesoscopic length scales [17,19-21,108,112-119]. This is very similar to the self-aggregation of surfactants in water. However, while in the surfactant case the aggregation is driven by the hydrophobicity of the alkyl chains, in the ILs the aggregation is driven by a combined effect of coulombic and van der Waals interactions.

The nano-structuring of ILs is revealed by a well-defined peak, typically found in the range of a few  $\text{nm}^{-1}$ , in the static structure factor ( $S(Q)$ ), determined for instance with X-ray or neutron scattering experiments, and modelled by MD simulations [17,19,20,112,117,119], see also Figure 10. Translating this peak into real space gives characteristic correlation lengths of 10 to 40 Å, which is remarkably large for a liquid. The heterogeneities are suggested to originate from a segregation of the alkyl chains, due to van der Waals interactions, into domains embedded into a charged matrix, see Figure 9. The size of the domains has been shown to depend linearly on the cation alkyl chain length [17,20], however, recent studies performed on relatively long alkyl chains ( $n > 12$ ) suggest a departure from this dependence [119]. In contrast, the use of different anions has a very weak effect on the polar domains in comparison with the changes caused in the charge alternation domains [120].

There is no doubt that the structure of some ILs is heterogeneous in nature where both polarity and charge alternation domains coexist, but the actual picture of how these structures are formed is still a question that remains unanswered. For instance, in ILs with short alkyl tails, i.e. weak van der Waals interactions, the coulombic interaction

are dominant, hence only the charge alternation prevails in the system as in the solvation model. However, as the alkyl chains are increased in length the van der Waals interaction start to play a more important role driving the aggregation of the chains, however the interactions that truly stabilize the system are of coulombic nature [121]. Further increase in the alkyl chain length can result in liquid crystalline behaviour, with the van der Waal interactions starting to dominate in the system [122], see Figure 9.

In an IL based electrolyte the presence of the  $\text{Li}^+$  is likely to induce different changes in mesoscopic structure depending on the kind of ordering on the system. For instance, in systems where the alkyl chains are relatively short, assuming the solvation model holds in this case, the presence of  $\text{Li}^+$  would induce changes in both the charge alternation domains as well as the polarity domains, which in this case would be a second solvation shell. Indeed in the paper V of this thesis we found that for the family of pyrrolidinium-based IL an alkyl chain  $n = 4$  will resemble a solvation model ordering, whereas for the imidazolium-based IL there will be already alkyl chain aggregation at the point. This finding underlines the importance of the choice of cations when searching for specific properties in ILs. Moreover, even more interesting is that the addition of Li-salt to systems with longer alkyl chains do not disrupt or modify the polarity domains, but actually enhanced the self-aggregation, in contrast to the effect in the charge alternation domains where considerably increase in characteristic size and order was found.

### 3.3 Dynamics in electrolytes

The ionic conductivity of an electrolyte can be expressed as

$$\sigma = \sum_i |n_i q_i \mu_i| \quad (3.1)$$

where  $n_i$  is the number of charge carriers,  $q_i$  is their net charge, and  $\mu_i$  is their mobility. From this equation is easy to see that if any of these parameters is increased the ionic conductivity will increase as well. However, in LIBs the charge of the carrier is fixed to one, hence increasing the numbers of carriers or their mobility are the only options. Furthermore, according to the Einstein relation, the mobility can be expressed as follows

$$\mu = \frac{q}{k_B T} D \quad (3.2)$$

where  $k_B$  is the Boltzmann constant,  $T$  the temperature, and  $D$  the diffusion constant.

If we make use of the Stokes-Einstein equation

$$D = \frac{k_B T}{6\pi\eta r} \quad (3.3)$$

and substitute it on the mobility equation we obtain

$$\mu = \frac{q}{6\pi\eta r} \quad (3.4)$$

where  $\eta$  is the dynamic viscosity of the medium and  $r$  is the radius of the spherical particle, here the effective radius of the ion diffusing. From here, it is clear that an increase in viscosity will decrease the mobility of the carriers and consequently the ionic conductivity.

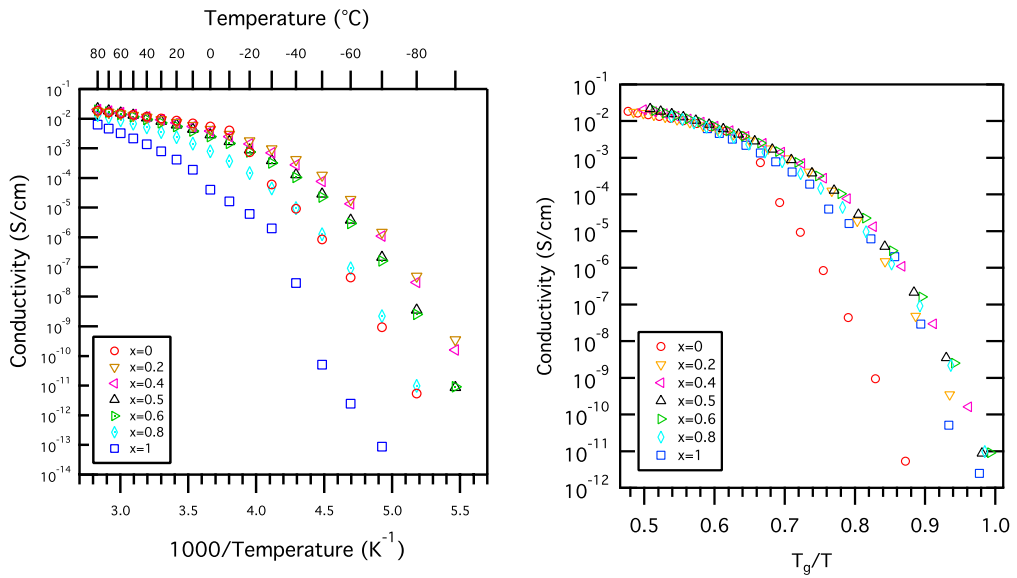
In liquid electrolytes the temperature dependence of the viscosity does not follow an Arrhenius behavior, but is instead better described by the Vogel-Tamman-Fulcher (VTF) function

$$\eta = \eta_0 \exp[BT_0/(T - T_0)]$$

where  $\eta_0$  is a constant,  $T_0$  is defined as the ideal glass transition temperature, and  $B$  is a constant related to the fragility of the material [123-125]. The term fragility is a measure of how much the temperature dependence of the viscosity deviates from the ideal Arrhenius behavior. A similar expression can be written for the ionic conductivity

$$\sigma = \sigma_0 \exp[BT_0/(T - T_0)]$$

where the parameters have equivalent meaning as in the viscosity equation.



x	0	0.2	0.4	0.5	0.6	0.8	1
$T_g(K)$	168	171	176	179	181	190	208

Figure 11. Left: Temperature dependence of the ionic conductivity of 0.8 molal LiTFSI in  $[EC:DMC(1:1)]_{(1-x)}[Pyr_{14}TFSI]_x$  mixtures. Right: Ionic conductivity of 0.8 molal LiTFSI  $[EC:DMC(1:1)]_{(1-x)}[Pyr_{14}TFSI]_x$  mixtures scaled to the glass transition temperatures. Data from paper IV of this thesis. Table: Glass transition temperature as a function a weight fraction of IL in the mixed electrolyte.

In Figure 11 the temperature dependence of the ionic conductivity in IL/organic solvent mixed electrolytes is shown as well as how the ionic conductivity scales with the glass transition temperature,  $T_g$ . It is clear that a reduction of temperature has a strong effect on the conductivity of the electrolytes. Also, it is possible to observe that variations in the glass transition temperature have a strong effect on the ionic conductivity. Moreover, the fact that the ionic conductivity perfectly scales with the glass transition temperature demonstrates that the transport mechanism is diffusive.

In standard electrolytes, the transport of the  $\text{Li}^+$  is dominated by diffusion; hence linear carbonates are used mainly to decrease the viscosity. However, as discussed in section 3.1.1 this approach might not be the ideal since different solvents might favor the existence of stable ion pairs and result in lower ionic conductivity. As the concentration of  $\text{Li}^+$  is increased, so is the viscosity, hence for many years the formulation of electrolytes has been optimized to balance the number of carriers and the viscosity.

The question that arises is if the transport mechanism at higher Li-salt concentrations is different. For instance, work performed by Yoshida et al. on solvated ILs, suggest that the  $\text{Li}^+$  transport mechanism might not be diffusive, but rather a Grotthuss-like mechanism where the  $\text{Li}^+$  is exchanged from one solvate to another [71]. Perhaps a similar behavior could also be envisaged in super-concentrated electrolytes, where the close proximity of the solvation shells allows for the  $\text{Li}^+$  to be transported from one site to another, without the need of the whole solvation shell to diffuse.

The transport properties in ILs have been extensively studied by means of NMR spectroscopy [126]. Despite the small size of the  $\text{Li}^+$ , the NMR measurements of a TFSI based IL show that in fact the  $\text{Li}^+$  possesses a lower diffusion coefficient ( $D_{\text{Li}} \approx 2 \cdot 10^{-7} \text{ cm}^2 \text{s}^{-1}$ ) compared to the other species in the IL based electrolyte ( $D_{\text{Cation}} \approx 7 \cdot 10^{-7} \text{ cm}^2 \text{s}^{-1}$  and  $D_{\text{Anion}} \approx 3 \cdot 10^{-7} \text{ cm}^2 \text{s}^{-1}$ ) [126]. The reason for this is that the  $\text{Li}^+$  is strongly coordinated to a pair of TFSI, which results in a rather large effective radius. Hence, a decrease of the diffusion coefficient is expected as predicted from the Stokes-Einstein equation. Work performed by Pitawala et al. has demonstrated that at low and intermediate Li-salt concentrations the ILs present diffusive transport properties as confirmed by the perfect scalability of the ionic conductivity with the glass transition temperature [64]. It is worth to mention that the effective radius of the  $\text{Li}^+$  can also be affected by being immersed in a highly ionic medium.

The presence of structural heterogeneities in ILs can in principle affect the diffusive motions of the ions. For instance, Martinelli et al. has found that changes in the alkyl chain lengths can invert the role of what ion diffuses faster in the IL [119]. Furthermore, recent studies by Araque et al. suggest that the nature of a solute has strong implications in the transport properties when dissolved in ILs with structural heterogeneities. For instance, neutral solutes will behave rather indifferently while traveling through charge alternation or alkyl chain domains, whereas charged solutes, like the  $\text{Li}^+$ , will experience a strong resistance when traveling through charge alternation domains as they become part of the charge matrix [127].

Regarding the dynamics present in ionic liquid at different length scales, i.e. charge alternation and polarity domains, Kofu et al. have provided an overall picture of the

relaxation processes involved [121,128,129]. Regarding the local dynamics, a fast relaxation process ca. 1 ps was assigned to the alkyl chain relaxation and was found to be independent of both alkyl chain length and anion type. Furthermore, a slower process ca. 10 ps was assigned to the relaxation of the imidazolium ring in a restricted area. The activation energy of the latter relaxation process was increased with the decrease of the anion size; however, it proved to be independent of the alkyl chain length. Furthermore, a structural relaxation process around 10-100ns was assigned to the polarity domains, and it was found to be dominated by coulombic interactions. The work of Kofu et al. has brought a very complete picture of the heterogeneous dynamics in ILs; however, our curiosity to investigate to what extent the substitution of the cation by Li<sup>+</sup> will affect such dynamics, as in the case of an IL based electrolyte, served as an motivation to perform the work in the paper VI. In the manuscript we reinforce the finding that introducing a more ionic species in the medium increases the activation energies in the system, drastically changing other properties like viscosity and glass transition.



# Chapter 4

## Experimental techniques

---

In this chapter a brief introduction to the experimental techniques is given. For each experimental technique a brief description of the measurements of interest and the basic theory behind is explained. Also some specifications on the sample preparation and the experimental setup will be provided.

### *4.1 Differential scanning calorimetry*

Differential scanning calorimetry (DSC) is one of the most widely used techniques for characterization of phase behavior and other thermal properties. DSC measures the energy changes that occur as a sample is heated, cooled, or held isothermally, together with the temperature at which these changes occur. These energy changes enable us to find and measure thermal transitions that occur in the sample quantitatively. With this information it is possible to characterize materials in terms of melting, glass transitions, crystallizations, and a range of more complex events. An advantage of DSC is that the sample preparation is very simple, usually with little or no preparation needed; therefore measurements can be made quickly and easily.

Figure 12 shows a typical DSC thermogram, where the most common transitions are depicted. The glass transition is represented as a step, whereas the melting and crystallization transitions are represented as peaks, but with different directions due to the nature of the transitions (exothermic or endothermic). Two different conventions exist to display the heat flow curve: one shows exotherms (release of energy from the system) in the downward direction and the other in the upward direction. In this thesis we will take the exotherms upward convention is applied.

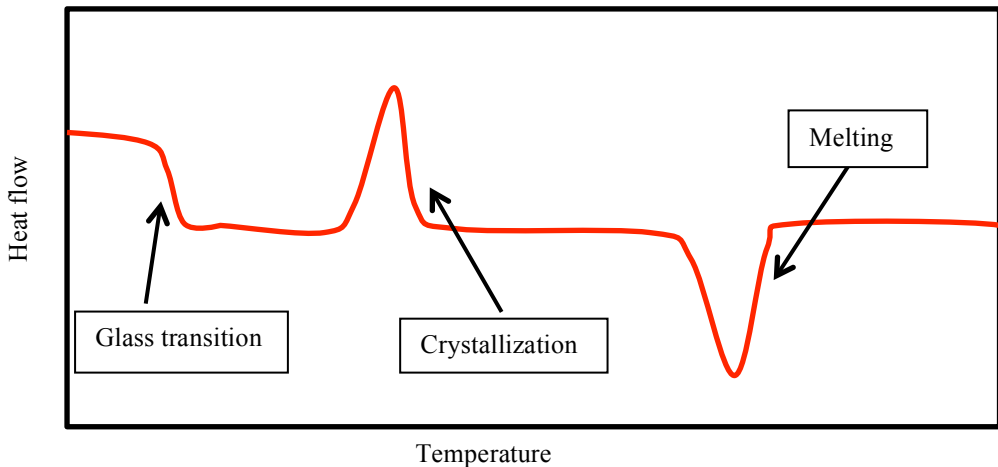


Figure 12. Typical DSC thermogram showing the glass transition, crystallization and melting processes.

The glass transition ( $T_g$ ) can occur over a region of temperatures, in some cases many tens of degrees. Because of this, it is important to specify how  $T_g$  was determined. There are several conventions, but the most widely used are the onset, midpoint, and endpoint of the glass transition. To define these three points, two tangents to the baselines are drawn (before and after the transition) then a tangent to the point of highest derivate during the transition is drawn, these three lines together will define the points of interest (see Figure 13). In this thesis, the onset convention is used. Regarding the crystallization ( $T_c$ ) and melting temperatures ( $T_m$ ), the values correspond to the peak position. For further information, the reader is suggested to consult the books in references [130-132].

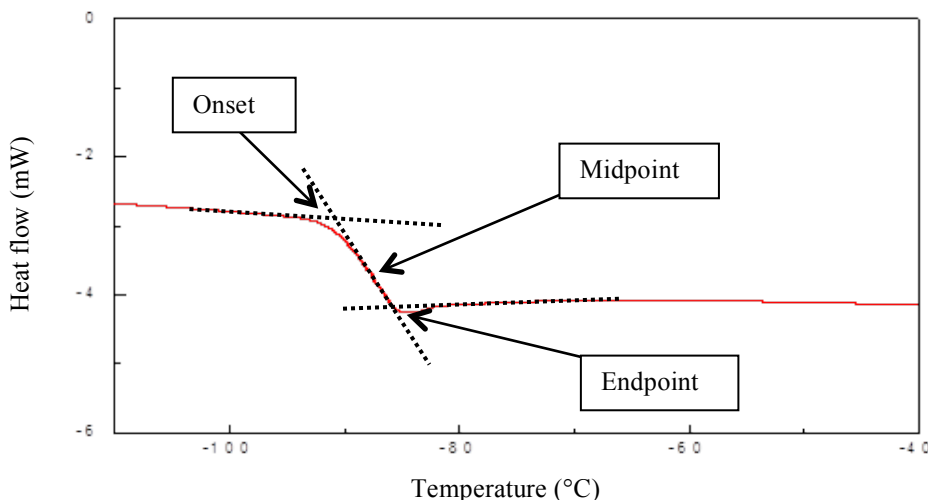


Figure 13. Glass transition and the three ways to define it: onset, midpoint and endpoint.

The experimental equipment used in this thesis work is a DSC-Q1000, TA Instruments. This equipment measures the heat flow as a function of temperature or time, where the actual value of heat flow measured depends upon a reference; therefore it is not absolute. The sample and reference are maintained at the same temperature throughout the experiment. The reference (in this case an empty aluminum pan) should have a well-defined heat capacity over the range of temperatures to be investigated.

## 4.2 Dielectric spectroscopy

Dielectric spectroscopy (DS), also known as impedance spectroscopy, measures the dielectric properties of a material by the interactions of an external field with the electric dipole moment of the material. DS measurements are often used for characterizing electrochemical systems, by means of measuring the impedance of a material over a range of frequencies. The term impedance is related to the opposition of flow of alternating current (AC) through a system. A passive electrical system comprises both an energy dissipator element, better known as a resistor, and energy storage element, known as a capacitor.

In the case of ionic conductivity measurements of electrolyte materials, the cells are usually made up of two identical cylindrical electrodes separated by a ring that contains the electrolyte, see Figure 14. The general approach is to apply an electrical field, in our case a voltage, to the electrodes and observe the response, in our case the resulting current. In most experiments it is always assumed that the properties of the electrode material are time-invariant, and therefore stable enough to determine other properties, as a function of temperature, oxygen partial pressure, applied hydrostatic pressure, or applied static voltage. A variety of microscopic processes can take place in the cell and together they lead to the overall electrical response.

### 4.2.1 Basic theory

When an electric field  $E$  is applied to a material, the charges and dipoles will reorient, resulting in a polarization  $P$  in the material. The relation between the applied electric field and the polarization of the material is given by

$$P = (\varepsilon_r - 1)\varepsilon_0 E \quad (4.1)$$

where  $\varepsilon_0$  and  $\varepsilon_r$  are the permittivity of the vacuum and the material respectively. Assuming that we are working in a linearly behaving, homogeneous, isotropic medium and knowing that the relation for the electrical displacement  $D$  is given by

$$D = \varepsilon_0 E + P \quad (4.2)$$

it is possible to rewrite  $D$  as a function of  $\varepsilon_r$  and  $E$  by substituting equation 4.1 into 4.2

$$D = \varepsilon_0 \varepsilon_r E \quad (4.3)$$

A modulated electrical field  $E_\omega(t) = E_0 \exp(i\omega t)$  will produce a modulated electric displacement, but with a phase difference due to the response time of the electric displacement  $D_\omega(t) = D_0 \exp(i\omega t - i\delta(\omega))$ . The ratio  $D_\omega/E_\omega$  is the complex dielectric permittivity, as a function of the frequency  $\omega$ .

$$\varepsilon^*(\omega) = \varepsilon'(\omega) - i\varepsilon''(\omega) = \frac{D(\omega)}{\varepsilon_0 E(\omega)} \quad (4.4)$$

If a modulated voltage is applied, a modulated current will be the response and as a result the complex impedance  $Z^*(\omega)$  can be obtained. From  $Z^*(\omega)$  it is possible to find the complex dielectric permittivity with the relationship

$$\varepsilon^*(\omega) = \frac{-i}{\omega C_0 Z^*(\omega)} \quad (4.5)$$

where  $C_0$  is the empty cell capacitance, which neglecting edge effects is equal to  $C_0 = \epsilon_0 A / l$  where  $A$  is the area and  $l$  is the distance between electrodes. With equation 4.5 it is possible to find the ionic conductivity by using the following relation [133]

$$\varepsilon^*(\omega) = \varepsilon'(\omega) + i \frac{\sigma}{\omega} \quad (4.6)$$

The dc-conductivity can be extracted by plotting the values of  $\sigma'(\omega)$  and taking the value of the plateau. If the  $\sigma'(\omega)$  is taken at several temperatures the dc-conductivity plot as a function of temperature is generated. For further information, the reader is suggested to consult the references [133].

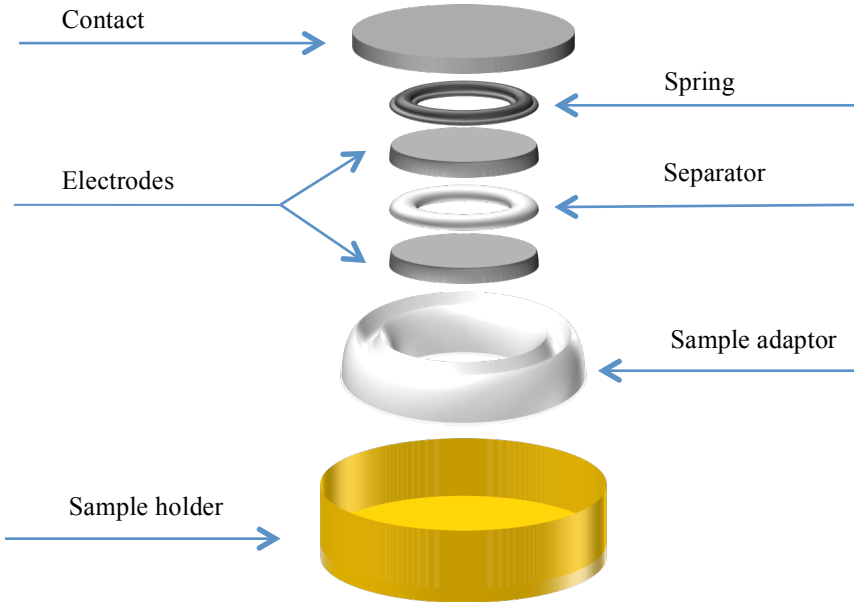


Figure 14. Schematic of dielectric spectroscopy sample container for liquid samples.

### 4.3 Raman Spectroscopy

Raman spectroscopy is a versatile technique, which nowadays is used in a wide range of applications such as pharmaceuticals, forensic science, polymer, and semiconductor industry, among others [94,134]. One of the main advantages of this technique, is that there is barely, or any, sample preparation needed, together with the facts that it is a non-invasive, and non-destructive technique. The Raman effect was independently discovered by C.V Raman [135] on liquids and L. Mandelstam [136] on crystals in 1928. However, A. Smekal predicted the basic principle already in 1923 [137]. Despite of the early studies of the effect, it was not until the advent of affordable laser systems that it became popular as a spectroscopy characterization technique.

When light interacts with a material it can be elastically or inelastically scattered. The former means that the incident and scattered light have identical energies, this phenomenon is known as Rayleigh scattering. The latter is the one that gives rise to the Raman effect, when the scattered light has an energy difference with respect to the incident light. This change in energy can come from interactions of different nature such as molecular vibrations (phonons) or other excitations in the system.

Depending on the nature of the interaction between the incoming photon and the sampled material, the inelastically scattered photons can have either higher or lower energy. In the former case, the affected molecule is in an excited vibrational state ( $E_1$ ) and after the interaction with the incoming photon it relaxes back to its ground state ( $E_0$ ). This is known as anti-Stokes scattering. In the second case, the molecule is in ground state ( $E_0$ ) and after interaction with the incoming photon it relaxes back to a state with higher energy ( $E_1$ ). This is known as Stokes scattering. In Figure 15 the scattering processes are schematically shown. In general, the number of molecules in the ground state is much higher than in the excited states and therefore, Stokes scattering is more intense. Yet, the total fraction of inelastically scattered light is still only a small portion compared to the Rayleigh scattered light ( $10^{-6}$ ).

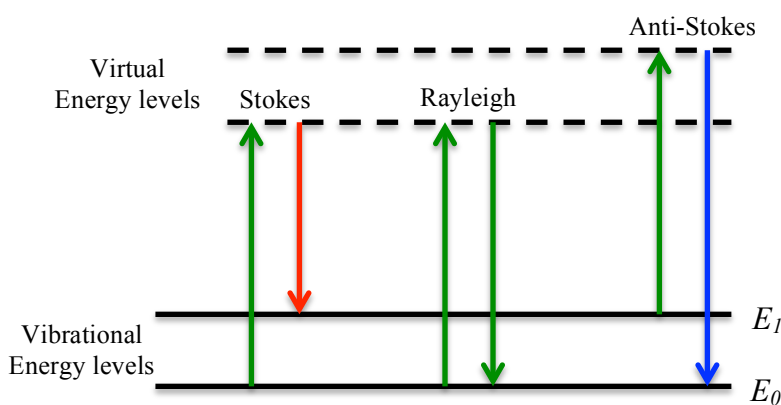


Figure 15. Energy level diagram for Stokes, Rayleigh and anti-Stokes scattering.

### 4.3.1 Classical treatment of the Raman effect

Even though the classical picture cannot fully describe the Raman effect, it gives a first insight into the basics of the scattering process. In the classical approach the system under study is regarded as collection of atoms undergoing simple harmonic vibrations and takes no account of the quantization of the vibrational energy. In a Raman experiment, monochromatic light of frequency ( $\nu_0$ ) can be described by its electric field ( $E$ )

$$E = E_0 \cos(2\pi\nu_0 t) \quad (4.7)$$

where  $E_0$  represents the amplitude of the electric field and  $t$  is the time. When a molecule interacts with the electric field, a dipole moment will be induced, i.e. the electrons are displaced relatively to its nuclei. For small electric fields, the induced dipole moment ( $p$ ) can be expressed as

$$p = \alpha E = \alpha E_0 \cos(2\pi\nu_0 t) \quad (4.8)$$

where  $\alpha$  is the polarizability of the molecule, or in other words how easy the electron cloud of a molecule can be distorted. If now we assume that the molecule is vibrating with frequency ( $\nu_s$ ), the displacement ( $q$ ) is given by

$$q = q_0 \cos(2\pi\nu_s t) \quad (4.9)$$

where  $q_0$  is the vibrational amplitude. For small amplitudes, the polarizability can be expressed as follows

$$\alpha = \alpha_0 + \left(\frac{d\alpha}{dq}\right) q \quad (4.10)$$

substituting equations (4.9) and (4.10) into (4.8), the polarizability can be re-written as

$$p = \alpha_0 E_0 \cos(2\pi\nu_0 t) + \left(\frac{d\alpha}{dq}\right) q_0 E_0 \cos(2\pi\nu_s t) \cos(2\pi\nu_0 t) \quad (4.11)$$

finally, reworking the previous expression with trigonometrical identities leads to

$$p = \alpha_0 E_0 \cos(2\pi\nu_0 t) + \frac{1}{2} \left(\frac{d\alpha}{dq}\right) q_0 E_0 \{\cos 2\pi(\nu_0 + \nu_s)t + \cos 2\pi(\nu_0 - \nu_s)t\} \quad (4.12)$$

In the above equation the first term represents the light scattered with frequency  $\nu_0$ , this is the Rayleigh scattering. The second term corresponds to Raman scattering with frequencies  $(\nu_0 + \nu_s)$ , anti-Stokes scattering, and  $(\nu_0 - \nu_s)$ , Stokes scattering. It is also observed that in order to have a Raman Scattering contribution at all the following relation has to be fulfilled

$$\left(\frac{d\alpha}{dq}\right) \neq 0 \quad (4.13)$$

or in plain words, in order for a molecule to be Raman active a change in the molecular polarization with respect to the vibrational coordinate is required. The

amount of the polarizability change determines the Raman scattering intensity. For further details of the Raman effect the reader is suggested to address the following books [138-140].

#### 4.3.2 Instrumental details and data treatment

The Raman spectroscopy instrument used during this thesis work is a Bruker MultiRAM Fourier Transform Raman (FT-Raman) spectrometer (see Figure 16). As the name states, it bases its principle of operating on the use of an interferometer in order to transform the scattered light into an interferogram, which is later Fourier Transformed to the Raman spectrum. A major advantage of this kind of equipment is the lower degree of interference of fluorescence with the spectrum due to the use of a Nd:YAG laser (1064 nm), due to the lower energy of the incoming photons. However, its Raman signal is rather weak given that the scattering intensity varies as  $\lambda^{-4}$  in comparison with the dispersive Raman equipment's that usually work with visible light. The equipment makes use of a liquid nitrogen cooled Ge-diode detector. For most of the experiments here reported, a resolution of  $2 \text{ cm}^{-1}$  full width at half maximum was used, but the system allows even better resolutions.

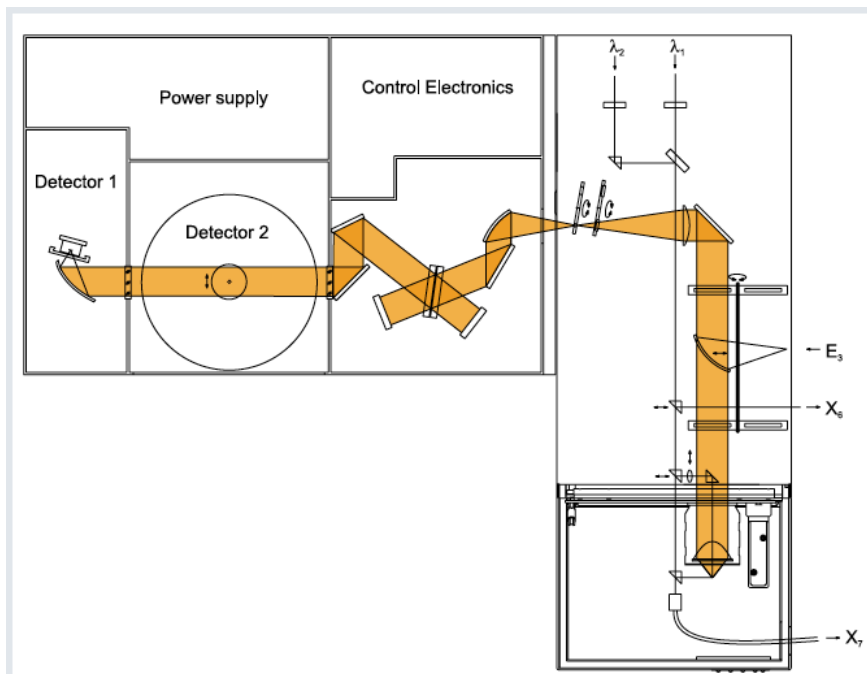


Figure 16. Schematic of the beam path of the Bruker Optics FT-Raman spectrometer (reprinted with permission of Bruker).

One of the strong points of Raman spectroscopy is the fact that quantitative and qualitative information can be obtained. However, in order to accurately obtain information from the spectra a fitting procedure is necessary. For this matter, we use the Voigt profile, which results from the convolution of a Gaussian and a Lorentzian profile.

$$V(x; \sigma, \gamma) = \int_{-\infty}^{\infty} G(x'; \sigma)L(x - x'; \gamma)dx' \quad (4.14)$$

here  $x$  is the frequency,  $G(x'; \sigma)$  is the centered Gaussian profile given by

$$G(x'; \sigma) = \frac{e^{-x'^2/(2\sigma^2)}}{\sigma\sqrt{2\pi}} \quad (4.15)$$

and  $L(x; \gamma)$  is the centered Lorentzian profile defined as follows

$$L(x; \gamma) = \frac{\gamma}{\pi(x^2 + \gamma^2)} \quad (4.16)$$

In order to efficiently compute the Voigt function in the fitting routine numerical approximations are used instead of the actual equations. If the reader wishes to learn more about the Voigt function and the fast computing approximations, the following references are suggested [141-145].

#### 4.4 Small Angle X-ray scattering

Small-angle X-ray scattering (SAXS), as the name suggests, is a scattering technique where monochromatic high-energy light (X-rays) is scattered from a sample and measured at low scattering angles with respect to the incident beam. The technique is generally used to study structures that can range from interatomic scales (nm) to macromolecular scales ( $\mu\text{m}$ ). With the advent of synchrotron radiation sources, the technique has become increasingly popular due to the reduced acquisition times and the accessible length scales in comparison with laboratory equipment [146].

##### 4.4.1 Basic theory

In Figure 17 the layout of a typical SAXS experiments is shown. A highly collimated and monochromatic X-ray beam of a given wavelength ( $\lambda$ ) impinges the sample and a two dimensional detector records the scattered light. In addition, the remaining unscattered/transmitted light is measured by a beamstop placed close to the detector.

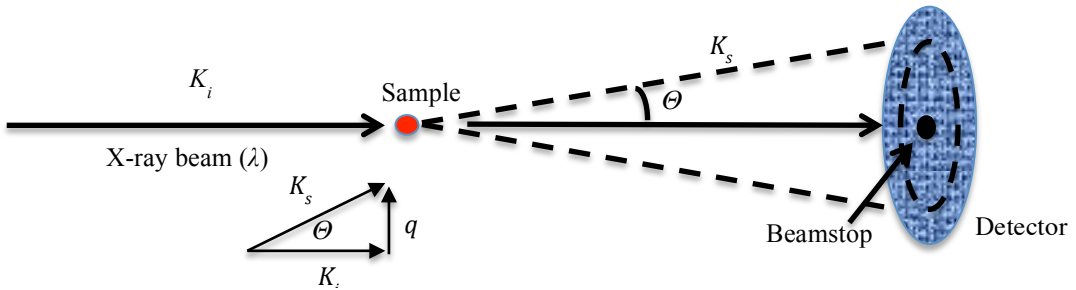


Figure 17. Schematic layout of a SAXS setup depicting the incident transmitted and scattered light, as well as the scattering vector ( $q$ ) definition.

In a SAXS experiment the number of photon as a function of scattering angle is measured. However, the number of photons detected strongly depends upon the incoming beam flux and the sample to detector distance, among other factors. For this reason the quantity of relevance in SAXS is the number of photons scattered into a given solid angle ( $\Omega$ ) normalized to the incoming photon flux. In addition it is

important to take into account the amount of light absorbed by the sample as well as the detector efficiency ( $\eta$ ). The former is easily obtained by introducing a transition coefficient ( $T_s$ ), which results from the ratio between the transmitted beam flux ( $I_t$ ), measured at the beamstop, and the incoming beam flux ( $I_0$ ), measured before the sample. The later is only dependent on the characteristics of the detector.

If we consider that the scattering process is elastic the magnitudes of incoming and scattered wave vectors should be equal,

$$|k_i| = |k_s| = \frac{2\pi}{\lambda} \quad (4.17)$$

The momentum transfer or scattering vector and its magnitude are defined as follows,

$$\mathbf{q} = k_s - k_i, \quad q = |\mathbf{q}| = \frac{4\pi}{\lambda} \sin(\theta/2) \quad (4.18)$$

With the above consideration, the measured intensity scattered from a sample ( $I_s$ ) as a function of momentum transfer  $\mathbf{q}$  can be expressed as:

$$I_s(\mathbf{q}) = I_0 A \Delta \Omega \eta T_s d_s \left( \frac{d\Sigma}{d\Omega} \right)_s (\mathbf{q}) \quad (4.19)$$

where  $A$  is the cross section of the beam,  $d_s$  is the sample thickness and  $d\Sigma/d\Omega$  is the differential scattering cross section.  $d\Sigma/d\Omega$  is expressed in  $\text{cm}^{-1}$  and contains information about the structure and interactions in the system and is obtained from the absolute calibration of the measured intensity [146].

#### 4.4.2 Instrumental details and data treatment

The SAXS experiments were performed in the MAX-lab at the Cassiopeia I911 beamline. The I911-4 is a new SAXS station, and uses a Si(111) crystal monochromator giving a wavelength of the incident beam of  $0.91\text{\AA}$ . A top view sketch of the Cassiopeia is shown in Figure 18. The size of the focal spot at the sample position, i.e. at 7 m from the monochromator, is about  $0.3 \times 0.2 \text{ mm}^2$  FWHM. The flux of the focused and collimated beam is estimated to be  $5 \times 10^{10}$  photons/s. The sample to detector distance can be changed from a few hundred millimeters to more than 2 meters. The accessible  $q$ -range of a typical I911-SAXS setup is  $0.01\text{\AA}^{-1}$ - $0.3\text{\AA}^{-1}$ . However, lower ( $0.006\text{\AA}^{-1}$ ) or higher ( $2\text{\AA}^{-1}$ ) values can be reached by changing the setup. The detector used in this system is a Pilatus 1M, and has the advantage of no dark currents or read out noise.

In order to effectively process data obtained from a SAXS experiment an appropriate calibration is needed. Among the available materials for calibration, here silver behenate (a well characterized material) was used to accurately determine the sample to detector distance, beam center and possible tilts of the detector by running a simply fitting routine. In addition, the use of a mask can be implemented to subtract possible artifacts such as dead pixels, the surrounding area close to the beam stop, and possible high intensity areas that are not inherent from the sample. With this procedure and the size of the pixels, a proper conversion of the two dimensional data into a  $I_s(\mathbf{q})$  vs  $\mathbf{q}$  plot can be done. The data were normalized to the incoming beam intensity and the

corresponding empty cell contribution was subtracted. However, calibration to absolute units was not performed. Once a proper  $I_s(\mathbf{q})$  vs  $\mathbf{q}$  plot was obtained the resulting curves were fitted with Lorentzian profiles in order to accurately determine the peak position, FWHM, etc.

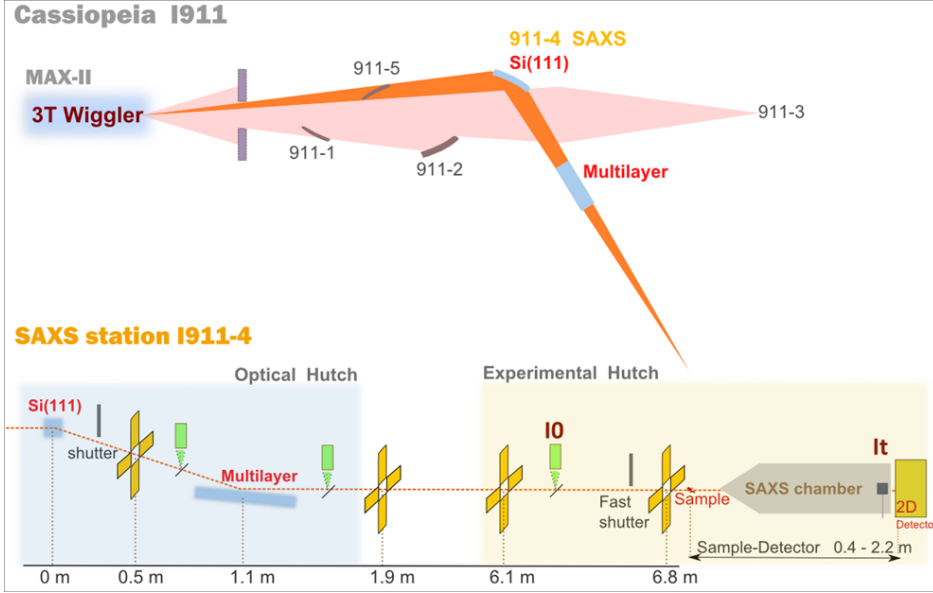


Figure 18. Top. Schematics from the wiggler indicating the part of the beam used for the I911-4 SAXS station. Bottom. Layout of the I911-4 optical and experimental hutches. (Figure reprinted with permission of Ana Labrador and Tomás Plivelic [147])

#### 4.5 Neutron Spin Echo

Neutron spin echo (NSE) spectroscopy is an inelastic neutron scattering technique introduced by Ferenc Mezei in the 1970s {mezei:1972io}. The spin echo spectrometer possesses an extremely high-energy resolution and directly measures the intermediate scattering function  $I(Q,t)$ , in contrast to other neutron scattering techniques where the dynamic structure factor  $S(Q,\omega)$  is measured instead. One of the unique features of NSE is the ability to study dynamics in the ps to ns time range on length scales from a few Å to several tens nm, thus covering the largest and longest time scales of all neutron spectrometers.

In inelastic neutron scattering the response of the sample is probed by the probability of a change in the neutron energy during the scattering process, and is expressed as the dynamic structure factor  $S(Q,\omega)$ . The resolution in the experiment is dependent on how precise the neutron energy, or velocity, change can be determined. Increasing the resolution typically means fewer neutrons, since neutrons with energies falling outside of the desired range are dismissed. As the intensity in the experiments decreases at least with the second power of the energy resolution, high-energy resolution experiments rapidly become intrinsically difficult due to the lack of signal.

The fundamental idea of NSE is to follow the energy change of each neutron in the scattering process. The existence of spin allows recording information of the neutron by using spin manipulations. A schematic of an instrumental setup is shown in Figure 19.

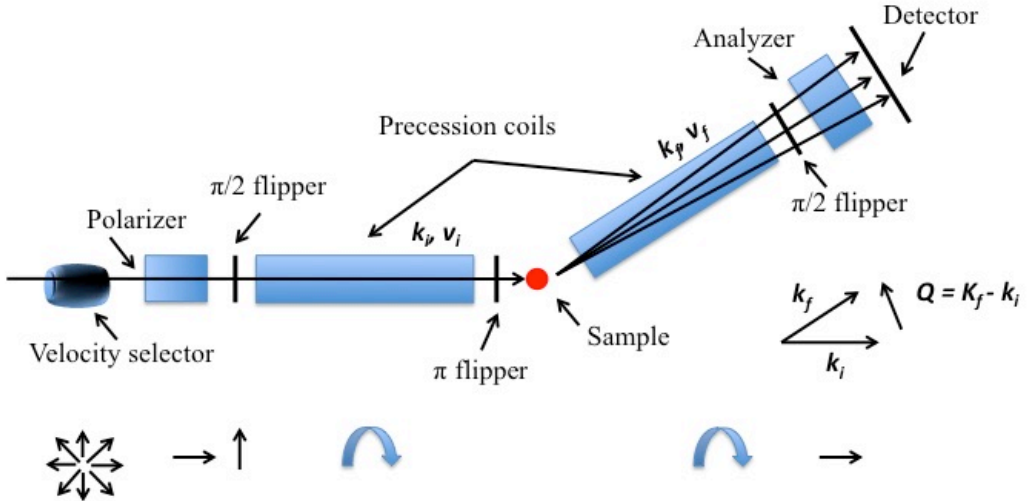


Figure 19. Schematic of the instrumental setup of a NSE spectrometer.

After passing through a velocity selector, the neutron beam is polarized parallel to the magnetic guide field. After this the neutron beam will impinge in a  $\pi/2$  flipper, which will flip the spins by  $90^\circ$  and initiate the Larmor precessions. The precession angle  $\varphi$  can be expressed by

$$\varphi = \frac{\gamma H l}{v} \quad (4.20)$$

where  $H$  is a magnetic field of variable strength inside the coils,  $l$  is the length of the coils and  $\gamma$  the Larmor constant, hence the precession angle records the velocity of the individual neutrons. Before reaching the sample a  $\pi$  flipper turns the spins  $180^\circ$  transforming  $\varphi$  to  $-\varphi$ .

Scattering within the sample results in a change of energy of the neutron. If we assume that the change in velocity is small we can approximate the energy change as follows

$$\hbar\omega = \frac{mv_f^2}{2} - \frac{mv_i^2}{2} \cong mv_i(v_f - v_i) \quad (4.21)$$

with a probability described by the dynamic structure factor  $S(Q,\omega)$ .

The momentum transfer  $Q$  can be expressed as

$$\hbar Q = mv_f - mv_i \quad (4.22)$$

After the neutron is scattered by the sample it goes through Lamor precessions in the second field  $\varphi'$ , which is added to the previous precession  $-\varphi$

$$-\varphi + \varphi' = -\frac{\gamma H l}{v_i} + \frac{\gamma H l}{v_f} \quad (4.23)$$

Since both the strength of the magnetic field and the length of the coil are equal and assuming small velocity changes we obtain

$$-\varphi + \varphi' = \gamma H l \left( \frac{1}{v_f} - \frac{1}{v_i} \right) \approx \gamma H l \frac{1}{v_i} (v_f - v_i) \quad (4.24)$$

substituting eq. 4.22 we obtain

$$-\varphi + \varphi' \approx \frac{\gamma H l}{mv_i^3} \hbar \omega \quad (4.25)$$

At the exit of the second coil the neutron impinges in another  $\pi/2$  flipper that turns the polarization parallel to the guide direction. Here, the transmission of the analyzer depends strongly on the polarization of the beam and we can obtain

$$P_x = \langle \cos(-\varphi + \varphi') \rangle = \langle \cos \frac{\gamma H l}{mv_i^3} \hbar \omega \rangle \quad (4.26)$$

where the average describes the probability distribution of  $\omega$ , this can be expressed by  $S(Q,\omega)$  and using the variable change

$$t = \frac{\gamma H l \hbar}{mv_i^3} \quad (4.27)$$

Using a proper normalization we obtain for the measured signal

$$P = \frac{\int S(Q,\omega) \cos(\omega t) d\omega}{\int S(Q,\omega) d\omega} \quad (4.28)$$

The nominator in eq. 4.29 is the cosine Fourier transform of  $S(Q,\omega)$ , i.e. the real part of the time dependent correlation function, or better known as the intermediate scattering function  $I(Q,t)$ . The denominator is just the static structure factor  $S(Q)$ , thus the directly observed result of a NSE experiment is

$$P = \frac{\text{Re} I(Q,t)}{S(Q)} \quad (4.29)$$

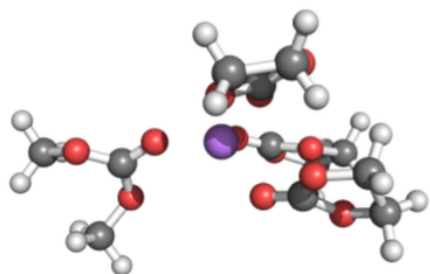
# Chapter 5

## Summary of appended papers

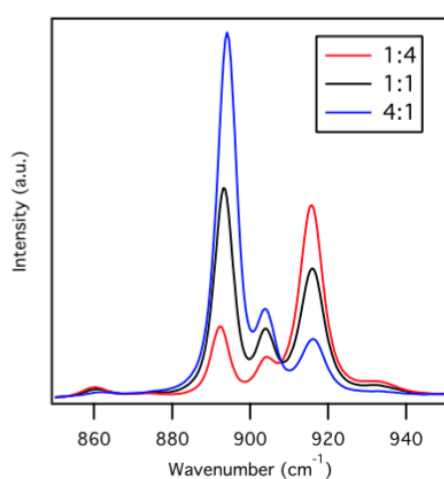
### Paper I

#### Solvation of Li<sup>+</sup> and Na<sup>+</sup> in carbonate based battery electrolytes – a combined computational and spectroscopy study

The solvation structure around the ions in electrochemical storage devices plays an important role in the overall performance of the system. Hence, the accurate determination of the explicit solvation shell is of great importance. To the date there are many discrepancies literature on how the solvation shell of currently used electrolyte is composed. Therefore, in this work the explicit solvation of both Li<sup>+</sup> and Na<sup>+</sup> has been studied with DFT and experimental techniques in neat cyclic (ethylene) and linear (dimethyl) carbonate solvents and their solvent mixtures. Our results show that the preferential solvation of the cations is considerably changed depending on the solvent composition. Moreover, we found that dimethyl carbonate in its cis-trans conformation takes a considerable contribution to the solvation of the cations when is in abundance.



Optimized structure of Li(EC)<sup>3</sup>(DMC)<sub>1</sub><sup>+</sup>

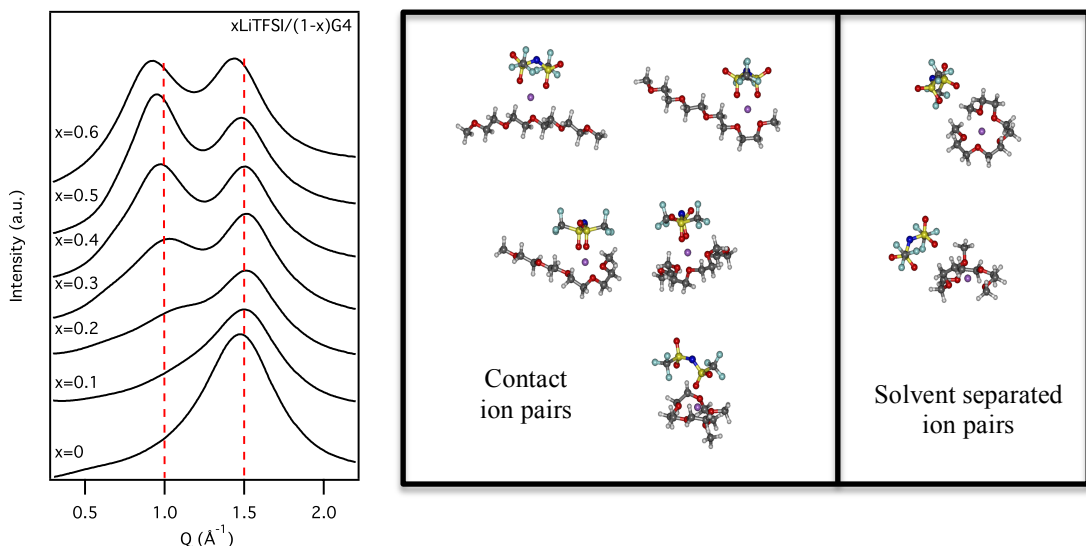


Raman spectra of 0.8 molar LiTFSI in EC:DMC with different weight ratios.

## Paper II

### A structural study of LiTFSI-tetraglyme mixtures: From diluted solutions to solvated ionic liquids

Solvated ionic liquids are an interesting alternative to traditional ionic liquids as electrolytes for Li-batteries. The concept is based on the formation of a complex between a cation and a solvent molecule effectively forming a large cationic species. When implementing this concept for Li-battery electrolytes a Li-based solvated ionic liquid can be realized by dissolving the right amount of a Li-salt in a solvent. In this work we report on the nano-structure of solvated ionic liquids formed by the equimolar mixture of LiTFSI and tetraglyme. Using small angle X-ray scattering as well as Raman spectroscopy and computational modeling we follow how the nano-structure develops as LiTFSI is added to the solvent. As the salt concentration is increased a peak ca.  $Q \approx 0.95 \text{ \AA}^{-1}$  grows in intensity, pointing out the presence of an ordering that resembles the alternation of charges in ionic liquids. With the assistance of computer modeling we show that this peak originates from the correlation between the  $\text{Li}^+$  and the center of mass of the  $\text{TFSI}^-$ . Moreover, we find that even at equimolar concentration not all  $\text{Li}^+$  are solvated by the tetraglyme, but a small fraction interacts directly with the TFSI.

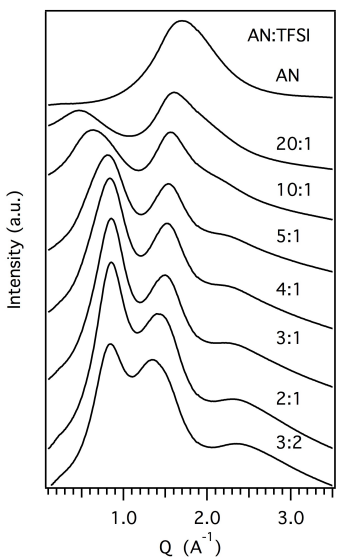


Left: SAXS diffraction patterns of different mole fractions of LiTFSI dissolved in G4. The dotted vertical lines represent guidelines to the eye. Right: Calculated energy minimum structures of the LiTFSI/G4 complexes.

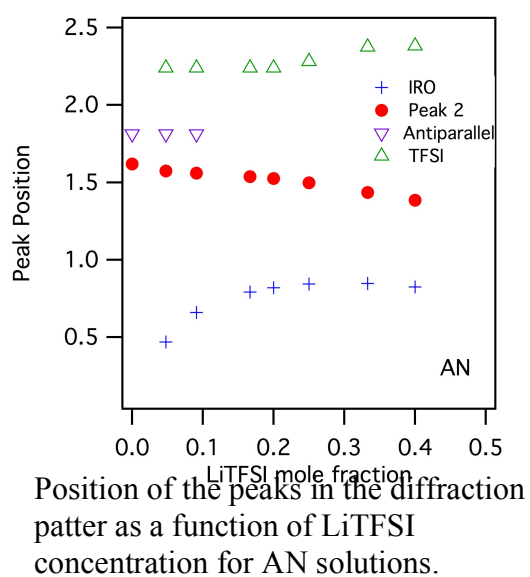
## Paper III

### Structure of super-concentrated LiTFSI in acetonitrile and propylene carbonate electrolytes

The use of super-concentrated electrolytes in lithium-ion batteries has gained considerable attention due to the increased electrochemical stability window and high rate capability. However, as the Li-salt concentration is increased many of the electrolyte properties change considerably as compared with standard formulations. For instance, the structure of highly concentrated solutions can be expected to be quite different from that found in ordinary liquids. In this work we address the issue of the nanostructure in highly concentrated electrolytes by means of small angle X-ray scattering. We have chosen to investigate highly concentrated solutions based on two different solvents propylene carbonate and acetonitrile, one asymmetric and one symmetric, respectively. We find that the symmetry of the solvent molecule plays an important role to induce an intermediate range order in the liquid. Our results suggest that in acetonitrile/LiTFSI solutions ordering of an extended solvation shell is observed at low salt concentrations, whereas in propylene carbonate/LiTFSI solutions only ordering related to the first solvation shell is observed. Furthermore, at high salt concentrations both systems show charge alternation ordering as the one typically found in ionic liquids. This results from the direct contact between first solvation shells.



SAXS diffraction patterns of AN/LiTFSI solutions at different concentration.

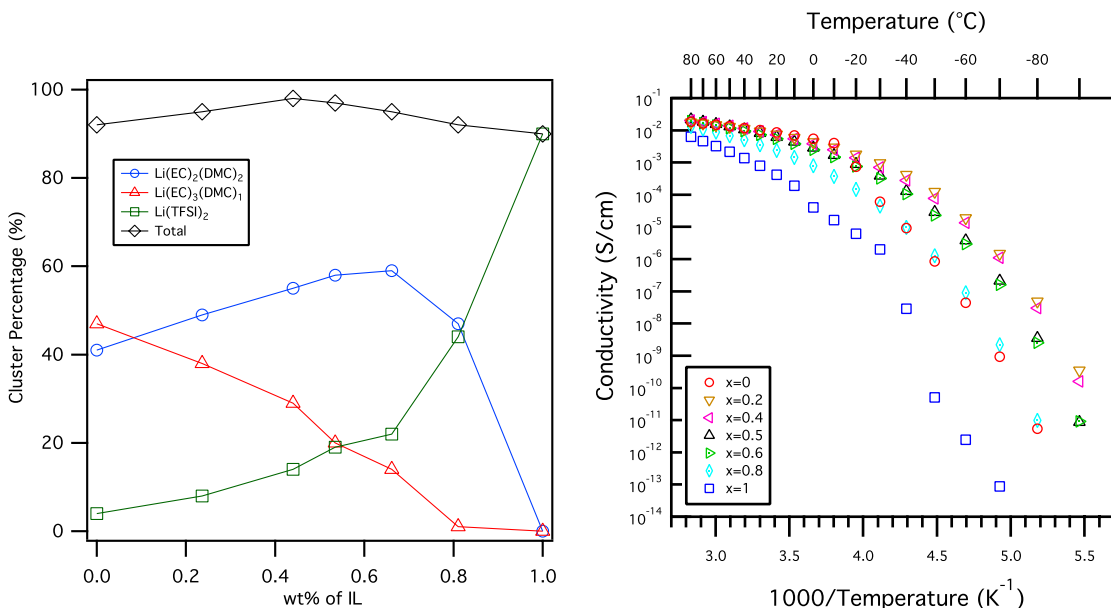


Position of the peaks in the diffraction pattern as a function of LiTFSI concentration for AN solutions.

## Paper IV

### Enhanced low-temperature ionic conductivity via different Li<sup>+</sup> solvated clusters in organic/ionic liquid mixed electrolytes

Safety is one of the primary concerns when it comes to the implementation of Li-batteries into electric vehicles. Hence, current electrolytes based on organic solvents and LiPF<sub>6</sub> pose a strong drawback in this regard. A viable solution is the inclusion of ionic liquids into the already optimized organic electrolytes. In this concept, advantage is taken from both, the low viscosity of organic solvents and the low flammability of the ILs. In this paper, a systematic study, ranging from a pure organic solvent to a pure IL based electrolyte, is performed by means of FT-Raman, DSC and dielectric spectroscopy. The average number of molecules/ions around each Li<sup>+</sup> points towards a more favorable solvation from the organic molecules. The progressive change between Li(TFSI)<sub>2</sub> clusters in the ionic liquid electrolyte to Li(EC)<sub>3</sub>(DMC)<sub>1</sub> and Li(EC)<sub>2</sub>(DMC)<sub>2</sub> clusters in the organic solvent electrolyte is revealed by our Raman measurements. The changes in the local configurations are also reflected in changes in the ionic conductivity and the phase behavior, where the formation of larger clusters lead to a decrease in the conductivity, whereas the presence of several different clusters at intermediate compositions effectively hinders the crystallization at low temperatures, which results in an enhanced low temperature ionic conductivity, in comparison with the neat ionic liquid or organic solvents electrolytes.



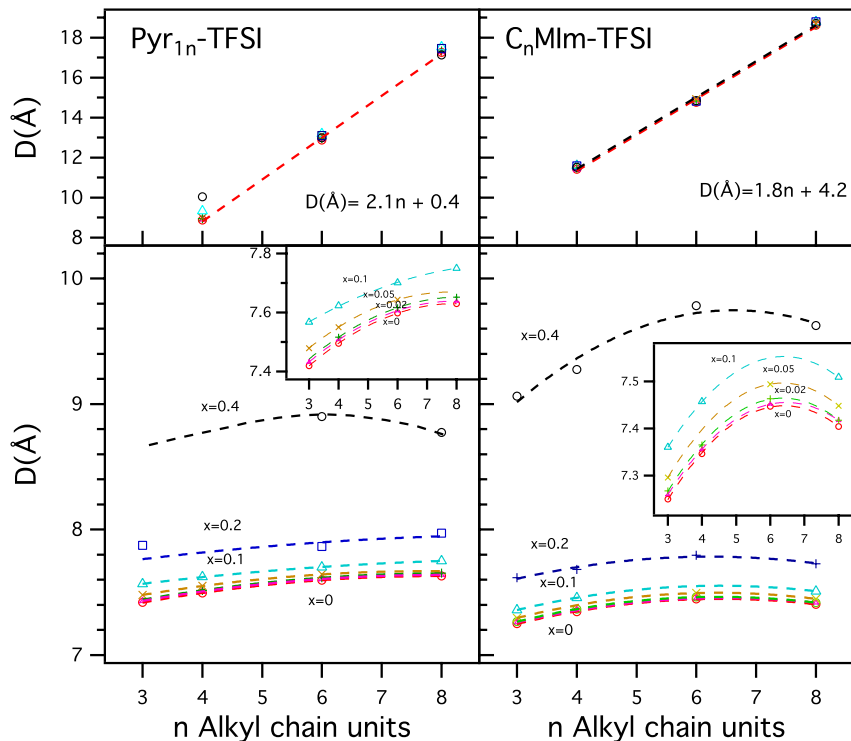
Fraction of possible configurations with the restriction that only triplets can contribute to the TFSI<sup>-</sup> coordination.

Temperature dependence of the ionic conductivity of the mixed electrolytes 0.8m LiTFSI in (1-x)(EC/DMC)/(xPYR<sub>14</sub>-TFSI).

## Paper V

### Effect of Lithium salt doping on the Nanostructure of Ionic Liquids

Ionic liquids, due to their ionic character and surfactant-like structure have structural order at mesoscopic scales, where other liquids remain homogeneous. There is general agreement that the long range ordering of ILs liquids come from the aggregation of the hydrophobic tails into mesoscopic domains. In this paper, we study the structural changes in two families of ionic liquids imidazolium and pyrrolidinium who share a common anion TFSI as a function of LiTFSI doping and alkyl chain length of the cation. We find that the correlation related to the clustering of alkyl chains is virtually unchanged, pointing towards a rather stable structural organization of the cations. However, the features correlated to the charge alternation of ions, is strongly affected by the addition of Li-salt, this is reflected as an increase in its characteristic length. From these results we interpret that the structural changes caused by the addition of Li-salt mostly reorganize the IL anion environment.

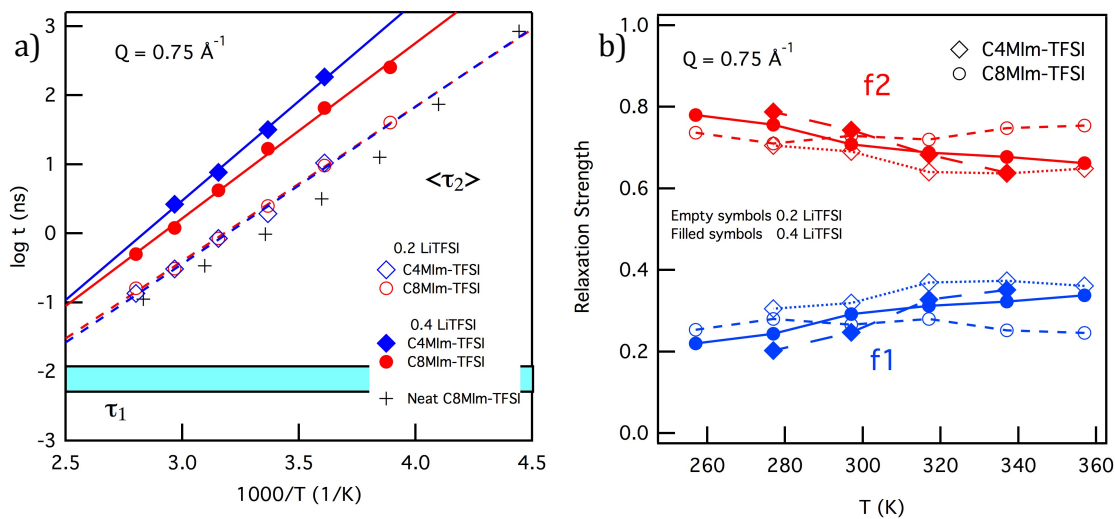


Characteristic distances of structural heterogeneities related to the pre-peak (top panels) and the charge alternation peak (bottom panels) in the static structure factor as a function of alkyl chain length  $n$  and Li salt concentration for  $\text{Pyr}_{1n}\text{-TFSI}$  (left) and  $\text{C}_n\text{MIm}\text{-TFSI}$  (right). Insets show a close up of the distances related to the charge alternation peak in the low salt concentration region.

## Paper VI

### Mesoscopic dynamics in lithium salt doped imidazolium based ionic liquids

An intriguing feature of ILs is the occurrence of structural heterogeneities on mesoscopic length scales (10-50 Å). The heterogeneities originate from the segregation of alkyl side chains on the cations into domains embedded in a charge matrix. On slightly shorter length scales, charge-ordering correlations are also present, resulting from the need of preserving charge neutrality. Both of these domains are expected to have a characteristic dynamical behaviour. In this work we reveal how the dynamics of the heterogeneities in ionic liquid electrolytes are influenced by the addition of the Li-salt, as well as the chain length of the cation. By means of neutron-spin echo spectroscopy we can follow at the dynamics on the relevant length and time scales. We found that the addition of Li-salt increases the activation energy of the dynamics related to both the relaxation in polarity domains and in the charge alternation domains suggesting that in both domains the dynamics are controlled by coulombic integrations. Furthermore, our results show that the presence of the Li-salt increases the self-aggregation of the alkyl chains, i.e. the polarity domains become more well defined, as well as well as their stability as a function of temperature as suggested by the increase in the relaxation strengths and their weaker temperature dependence in comparison with neat ionic liquids.



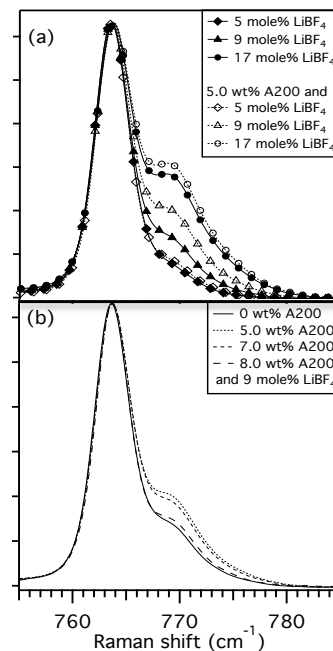
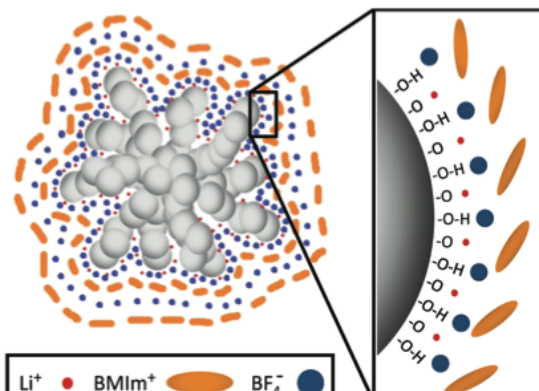
Results of the fitting of  $I(Q,t)/I(Q,0)$  for  $(1-x)CnMIm\text{-TFSI}/xLiTFSI$  ( $n=4,8$  and  $x=0.2,0.4$  at  $Q=0.75 \text{ \AA}^{-1}$ ). (a) Arrhenius plot of the relaxation times. (b) Temperature dependence of the relaxation strengths.

## Paper VII

### Effect of lithium salt on the stability of dispersions of fumed silica in the ionic liquid BMImBF<sub>4</sub>

In this paper we investigate the effect of Li-salt doping on the stability of colloidal dispersions. Fumed silica is known to form stable suspension in water, however the mechanisms that stabilize this kind of systems in ionic liquids is still a subject of discussion. Dispersions of fumed silica, Aerosil 200, and the ionic liquid 1-butyl-3-methylimidazolium tetraflouroborate (BMImBF<sub>4</sub>) as a function of the Li-salt concentration with the same anion. A systematic study by Photon correlation spectroscopy was performed to follow the aggregation behavior at low silica concentrations, whereas Raman spectroscopy was used to investigate the interactions of the ionic liquid and with the silica surface. We find that the addition of Li-salt increases the stability of the suspensions, with smaller agglomerates of silica particles and higher gelation concentrations. The increased stability with the addition of Li salt is explained by the formation of a more stable solvation layer, where Li ions accumulate on the surface of the silica nanoparticles and strengthen the interaction between them and the BF<sub>4</sub> anions, as suggested by Raman spectroscopy. Upon gelation, the silica nanoparticles hydrogen bond to each other and effectively expels the lithium ions from the surface.

Model for the solvation shell around the Aerosil 200 particle in LiBF<sub>4</sub>-doped BMImBF<sub>4</sub>.



(a) Symmetric stretch mode of the BF<sub>4</sub> anion in BMImBF<sub>4</sub> with different concentrations of LiBF<sub>4</sub> (filled symbols) and with the addition of 5.0 wt % Aerosil 200 (open symbols). (b) Symmetric stretch mode of the BF<sub>4</sub> anion for 9.0 mol % LiBF<sub>4</sub> in BMImBF<sub>4</sub> with different concentrations of Aerosil 200. The concentration of Aerosil 200 is varied around the gelation concentration: 5.0 wt % is a colloidal dispersion; 7.0 wt % is a weak gel; and 8.0 wt % is a strong gel.



## Outlook

---

Lithium-ion batteries are rapidly finding their way into the electric vehicle market. However, in order to become a fully accepted technology by society breakthroughs need to be done not only on performance but also on safety aspects. In this thesis, much effort was invested in determining the solvation structure of the different electrolytes and how these structures correlate with macroscopic properties of the system. However, there are still many open questions regarding the transport mechanism in the systems as well as what are the true limiting factors in each of them. For instance, in the case of super-concentrated electrolytes the life-time of the solvation shell could be directly related to the high rate capability of these systems. Moreover, the effect of the extended solvation shell found in the acetonitrile system could have strong implications at intermediate salt concentrations. Furthermore, the presence of structure heterogeneities of ionic liquids could be a devastating effect in the diffusion motion of the ions, but perhaps less detrimental if other transport mechanism is present. In short, the dynamic behavior of these new concept electrolyte sis still unknown and worth to out attention on.

Moreover, the challenges are not only present in the studied systems, but also on the required techniques to fully characterized them. We have recently focus on the methodology development to be able to use X-ray photon correlation spectroscopy (XPCS) in our electrolytes. While neutron scattering techniques give us access to times scales up to tens of ns XPCS can push the time experimental window all the way to seconds. However, due to the required long acquisition times and the high intensity of the beam, our measurements are unrealizable due to radiation damage. Hence we are developing a method based on the split-and-delay line approach for X-ray free electron lasers to address this issue. This approach is based on the analysis of photon-event-probabilities and can be used for extremely weak scattering patterns allowing a major reduction in exposure times and deposited dose in the sample.

## Acknowledgments

---

First of all, I would like to express my appreciation to my supervisor Professor Aleksandar Matic who on a regular basis provide me with scientific and moral support. Thus, I consider him not only a good influence in my career but also a good friend.

I would like to thank all the group members of Condensed Matter Physics for their continuous support and great environment provided, with special attention to Damien Monti for his persistent efforts to always compile the best of 9gag for me. I would also like to express my gratitude to Ezio Zanghellini for enabling science on the lab and the valuable support provided every time it was needed. I would also like to thank Professor Gunnar Westman for allowing me to experience the life of a chemist for a short period of time.

Last but not least, I would like to thank my family for their unconditional support and encouragement during everyday of my life. I would like to express my gratitude to all the friends I have meet during my stay in Sweden, with special attention to those ones of Balkan origins, Calle, and Massi, without you my journey through this PhD would not have the same flavor.

## Bibliography

---

- [1] B. Scrosati and J. Garche, *Journal of Power Sources* **195**, 2419 (2010).
- [2] J. M. Tarascon and M. Armand, *Nature* **414**, 359 (2001).
- [3] A. Hammami, N. Raymond, and M. Armand, *Nature* **424**, 635 (2003).
- [4] S. S. Zhang, *Journal of Power Sources* **162**, 1379 (2006).
- [5] A. von Cresce and K. Xu, *J. Electrochem. Soc.* (2011).
- [6] Y. Yamada, M. Yaegashi, T. Abe, and A. Yamada, *Chem. Commun.* **49**, 11194 (2013).
- [7] Y. Yamada, K. Furukawa, K. Sodeyama, K. Kikuchi, M. Yaegashi, Y. Tateyama, and A. Yamada, *J. Am. Chem. Soc.* **136**, 5039 (2014).
- [8] Y. Kameda, Y. Umebayashi, M. Takeuchi, M. A. Wahab, S. Fukuda, S.-I. Ishiguro, M. Sasaki, Y. Amo, and T. Usuki, *J. Phys. Chem. B* **111**, 6104 (2007).
- [9] K. Ueno, K. Yoshida, M. Tsuchiya, N. Tachikawa, K. Dokko, and M. Watanabe, *J. Phys. Chem. B* **116**, 11323 (2012).
- [10] S. Seki, Y. Ohno, Y. Kobayashi, H. Miyashiro, A. Usami, Y. Mita, H. Tokuda, M. Watanabe, K. Hayamizu, S. Tsuzuki, M. Hattori, and N. Terada, *Journal of Power Sources* **243**, 323 (2013).
- [11] M. Nie, D. P. Abraham, D. M. Seo, Y. Chen, A. Bose, and B. L. Lucht, *J. Phys. Chem. C* **117**, 25381 (2013).
- [12] Y. Yamada, K. Furukawa, K. Sodeyama, K. Kikuchi, M. Yaegashi, Y. Tateyama, and A. Yamada, *J. Am. Chem. Soc.* **136**, 5039 (2014).
- [13] B. Rezaei, S. Mallakpour, and M. Taki, *Journal of Power Sources* **187**, 605 (2009).
- [14] P. M. Bayley, A. S. Best, D. R. MacFarlane, and M. Forsyth, *J. Power Sources* **13**, 4632 (2011).
- [15] T. Sato, T. Maruo, S. Marukane, and K. Takagi, *Journal of Power Sources* **138**, 253 (2004).
- [16] A. Lewandowski and A. Świderska-Mocek, *Journal of Power Sources* **194**, 601 (2009).
- [17] O. Russina, A. Triolo, L. Gontrani, and R. Caminiti, *J. Phys. Chem. Lett.* **3**, 27 (2012).
- [18] L. Aguilera, J. Völkner, A. Labrador, and A. Matic, *Phys. Chem. Chem. Phys.* **17**, 27082 (2015).
- [19] O. Russina and A. Triolo, *Faraday Discuss.* **154**, 97 (2011).
- [20] A. Triolo, O. Russina, H.-J. Bleif, and E. Di Cola, *J. Phys. Chem. B* **111**, 4641 (2007).

- [21] H. K. Kashyap, J. J. Hettige, H. V. R. Annapureddy, and C. J. Margulis, *Chem. Commun. (Camb.)* **48**, 5103 (2012).
- [22] J. J. Hettige, H. K. Kashyap, H. V. R. Annapureddy, and C. J. Margulis, *J. Phys. Chem. Lett.* **4**, 105 (2013).
- [23] D. Linden and T. Reddy, *Handbook of Batteries (Mcgraw-Hill Handbooks)*, 3rd ed. (McGraw-Hill Professional, 2001).
- [24] M. Armand and J. M. Tarascon, *Nature* **451**, 652 (2008).
- [25] B. Scrosati, *J Solid State Electrochem* **15**, 1623 (2011).
- [26] S. Wilken, P. Johansson, and P. Jacobsson, *Solid State Ionics* **225**, 608 (2012).
- [27] K. Xu, *Chem. Rev.* **104**, 4303 (2004).
- [28] T. Nagaura and K. Tozawa, *Progresss in Batteries and Solar Cells* **9**, 209 (1990).
- [29] R. P. Seward and E. C. Vieira, *J. Electrochem. Soc.* **142**, 3465 (1995).
- [30] R. Fong, U. von Sacken, and J. R. Dahn, *Chem. Rev.* **104**, 4535 (2004).
- [31] E. Peled, *J. Electrochem. Soc.* **126**, 2047 (1979).
- [32] Y. Nishi, N. Azuma, and A. Omaru, (25 September 1990).
- [33] J. M. Tarascon and D. Guyomard, *Solid State Ionics* **69**, 293 (1994).
- [34] H. Yang, G. V. Zhuang, and P. N. Ross Jr., *Journal of Power Sources* **161**, 573 (2006).
- [35] S. Wilken, M. Treskow, J. Scheers, P. Johansson, and P. Jacobsson, *RSC Adv.* **3**, 16359 (2013).
- [36] C. Arbizzani, G. Gabrielli, and M. Mastragostino, *Journal of Power Sources* **196**, 4801 (2011).
- [37] T. Kawamura, A. Kimura, M. Egashira, S. Okada, and J.-I. Yamaki, *Journal of Power Sources* **104**, 260 (2002).
- [38] G. G. Botte, R. E. White, and Z. Zhang, *Journal of Power Sources* **97-98**, 570 (2001).
- [39] Y. Yamada and A. Yamada, *J. Electrochem. Soc.* **162**, A2406 (2015).
- [40] J. Wang, Y. Yamada, K. Sodeyama, C. H. Chiang, Y. Tateyama, and A. Yamada, *Nat Commun* **7**, 12032 (2016).
- [41] K. Ueno, J.-W. Park, A. Yamazaki, T. Mandai, N. Tachikawa, K. Dokko, and M. Watanabe, *J. Phys. Chem. C* **117**, 20509 (2013).
- [42] D. M. Seo, D. M. Seo, O. Borodin, O. Borodin, D. Balogh, D. Balogh, M. O'Connell, M. O'Connell, Q. Ly, Q. Ly, S.-D. Han, S. D. Han, S. Passerini, S. Passerini, W. A. Henderson, and W. A. Henderson, *J. Electrochem. Soc.* **160**, A1061 (2013).
- [43] A. N. Dey and B. P. Sullivan, *J. Electrochem. Soc.* **117**, 222 (1970).
- [44] I. A. Shkrob, Y. Zhu, T. W. Marin, and D. Abraham, *J. Phys. Chem. C* **117**, 19255 (2013).
- [45] M. W. Rupich, L. Pitts, and K. M. Abraham, *J. Electrochem. Soc.* **129**, 1857 (1982).
- [46] K. Yoshida, M. Tsuchiya, N. Tachikawa, K. Dokko, and M. Watanabe, *J. Phys. Chem. C* **115**, 18384 (2011).
- [47] M. Freemantle, *An Introduction to Ionic Liquids* (Royal Society of Chemistry, 2010).
- [48] C. P. Fredlake, J. M. Crosthwaite, D. G. Hert, S. N. V. K. Aki, and J. F. Brennecke, *J. Chem. Eng. Data* **49**, 954 (2004).
- [49] Y. U. Paulechka, D. H. Zaitsau, G. J. Kabo, and A. A. Strechan, *Thermochimica Acta* **439**, 158 (2005).

- [50] O. Aschenbrenner, S. Supasitmongkol, M. Taylor, and P. Styring, *Green Chem.* **11**, 1217 (2009).
- [51] H. Nakagawa, Y. Fujino, S. Kozono, Y. Katayama, T. Nukuda, H. Sakaeb, H. Matsumoto, and K. Tatsumi, *Journal of Power Sources* **174**, 1021 (2007).
- [52] G. B. Appetecchi, M. Montanino, A. Balducci, S. F. Lux, M. Winterb, and S. Passerini, *Journal of Power Sources* **192**, 599 (2009).
- [53] A. Stoppa, O. Zech, W. Kunz, and R. Buchner, *J. Chem. Eng. Data* **55**, 1768 (2010).
- [54] Y.-H. Yu, A. N. Soriano, and M.-H. Li, *Thermochimica Acta* **482**, 42 (2009).
- [55] Q. X. Liu, S. Z. El Abedin, and F. Endres, *Surface and Coatings Technology* **201**, 1352 (2006).
- [56] S. Caporali, A. Fossati, A. Lavacchi, I. Perissi, A. Tolstogouzov, and U. Bardi, *J. Electrochem. Soc.* **152**, A2327 (2005).
- [57] P. Wasserscheid and W. Keim, *Angewandte Chemie* (2000).
- [58] D. Zhao, M. Wu, Y. Kou, and E. Min, *Catalysis Today* **74**, 157 (2002).
- [59] M. Armand, F. Endres, D. R. MacFarlane, H. Ohno, and B. Scrosati, *Nat Mater* **8**, 621 (2009).
- [60] M. Gorlov and L. Kloo, *Dalton Trans.* 2655 (2008).
- [61] H. Nakamoto, A. Noda, K. Hayamizu, S. Hayashi, H. Hamaguchi, and M. Watanabe, *J. Phys. Chem. C* **111**, 1541 (2007).
- [62] L. Damen, M. Lazzari, and M. Mastragostino, *Journal of Power Sources* **196**, 8692 (2011).
- [63] H. Sakaeb, H. Matsumoto, and K. Tatsumi, *Electrochimica Acta* **53**, 1048 (2007).
- [64] J. Pitawala, J.-K. Kim, P. Jacobsson, V. Koch, F. Croce, and A. Matic, *Faraday Discuss.* **154**, 71 (2011).
- [65] A. Martinelli, A. Matic, P. Jacobsson, L. Börjesson, A. Fericola, and B. Scrosati, *J. Phys. Chem. B* **113**, 11247 (2009).
- [66] P. Johansson, S. P. Gejji, J. Tegenfeldt, and J. Lindgren, *Electrochimica Acta* **43**, 1375 (1998).
- [67] H. Tokuda, S. Tsuzuki, M. A. B. H. Susan, K. Hayamizu, and M. Watanabe, *J. Phys. Chem. B* **110**, 19593 (2006).
- [68] C. A. Angell, *J. Electrochem. Soc.* **112**, 1224 (1965).
- [69] C. A. Angell, Y. Ansari, and Z. Zhao, *Faraday Discuss.* **154**, 9 (2012).
- [70] T. Tamura, K. Yoshida, T. Hachida, M. Tsuchiya, M. Nakamura, Y. Kazue, N. Tachikawa, K. Dokko, and M. Watanabe, *Chem. Lett.* **39**, 753 (2010).
- [71] K. Yoshida, M. Nakamura, Y. Kazue, N. Tachikawa, S. Tsuzuki, S. Seki, K. Dokko, and M. Watanabe, *J. Am. Chem. Soc.* **133**, 13121 (2011).
- [72] J.-A. Choi, E.-G. Shim, B. Scrosati, and D.-W. Kim, *Biotechnol. Bioeng.* **94**, 473 (2006).
- [73] R.-S. Kühnel, N. Böckenfeld, S. Passerini, M. Winter, and A. Balducci, *Electrochimica Acta* **56**, 4092 (2011).
- [74] L. Lombardo, S. Brutti, M. A. Navarra, S. Panero, and P. Reale, *Journal of Power Sources* **227**, 8 (2013).
- [75] C. Locati, U. Lafont, C. J. Peters, and E. M. Kelder, *Journal of Power Sources* **189**, 454 (2009).
- [76] M. Moshkovich, M. Cojocaru, H. E. Gottlieb, and D. Aurbach, *J. Electroanal Chem* **497**, 84 (2001).

- [77] J. S. Gnanaraj, E. Zinigrad, L. Asraf, H. E. Gottlieb, M. Sprecher, M. Schmidt, W. Geissler, and D. Aurbach, *J. Electrochem. Soc.* **150**, (2003).
- [78] W. Kong, H. Li, X. Huang, and L. Chen, *Journal of Power Sources* **142**, 285 (2005).
- [79] G. H. Lane, A. S. Best, D. R. MacFarlane, M. Forsyth, P. M. Bayley, and A. F. Hollenkamp, *Electrochimica Acta* **55**, 8947 (2010).
- [80] P. M. Bayley, G. H. Lane, N. M. Rocher, B. R. Clare, A. S. Best, D. R. MacFarlane, and M. Forsyth, **11**, 7202 (2009).
- [81] P. Muller, *Pure and Applied Chemistry* **66**, 1077 (1994).
- [82] I. Skarmoutsos, V. Ponnuchamy, V. Vetere, and S. Mossa, *J. Phys. Chem. C* **119**, 4502 (2015).
- [83] J. Pitawala, A. Martinelli, P. Johansson, P. Jacobsson, and A. Matic, *Journal of Non-Crystalline Solids* **407**, 318 (2015).
- [84] R. D. Green and N. Sheppard, *J. Chem. Soc., Faraday Trans. 2* **68**, 821 (1972).
- [85] X. Bogle, R. Vazquez, S. Greenbaum, A. V. W. Cresce, and K. Xu, *J. Phys. Chem. Lett.* **4**, 1664 (2013).
- [86] K. Matsubara, R. Kaneuchi, and N. Maekita, *Faraday Trans.* **94**, 3601 (1998).
- [87] S.-A. Hyodo and K. Okabayashi, *Electrochimica Acta* **34**, 1551 (1989).
- [88] R. D. ShannonIUCr, *Acta Crystallogr Sect a Cryst Phys Diffraction Gen Crystallogr* **32**, 751 (1976).
- [89] R. D. Shannon and C. T. Prewitt, *Acta Cryst* (1969). B25, 925-946 (1969).
- [90] O. Borodin and G. D. Smith, *J. Phys. Chem. B* **113**, 1763 (2009).
- [91] R. Aroca, M. Nazri, G. A. Nazri, A. J. Camargo, and M. Trsic, *J Solution Chem* **29**, 1047 (2000).
- [92] P. Johansson, *J. Phys. Chem. A* **105**, 9258 (2001).
- [93] A. Martinelli, A. Matic, and P. Johansson, *Journal of Raman Spectroscopy* **42**, 522 (2011).
- [94] J. C. Lassègues, J. Grondin, R. Holomb, and P. Johansson, *J. Raman Spectrosc.* **38**, 551 (2007).
- [95] I. Rey, P. Johansson, J. Lindgren, J. C. Lassègues, J. Grondin, and L. Servant, *J. Phys. Chem. A* **102**, 3249 (1998).
- [96] M. Herstedt, M. Smirnov, P. Johansson, M. Chami, J. Grondin, L. Servant, and J. C. Lassègues, *J. Raman Spectrosc.* **36**, 762 (2005).
- [97] O. Borodin and G. D. Smith, *J. Phys. Chem. B* **110**, 4971 (2006).
- [98] D. M. Seo, O. Borodin, S. D. Han, P. D. Boyle, and W. A. Henderson, *J. Electrochem. Soc.* **159**, A1489 (2012).
- [99] D. W. McOwen, D. M. Seo, O. Borodin, J. Vatamanu, P. D. Boyle, and W. A. Henderson, *Energy Environ. Sci.* **7**, 416 (2014).
- [100] H. Shobukawa, H. Tokuda, S.-I. Tabata, and M. Watanabe, *J. Am. Chem. Soc.* **128**, 6636 (2006).
- [101] Z. Li, G. D. Smith, and D. Bedrov, *J. Phys. Chem. B* **116**, 12801 (2012).
- [102] Y. Umebayashi, T. Mitsugi, S. Fukuda, T. Fujimori, K. Fujii, R. Kanzaki, M. Takeuchi, and S.-I. Ishiguro, *J. Phys. Chem. B* **111**, 13028 (2007).
- [103] J.-C. Lassègues, J. Grondin, and D. Talaga, **8**, 5629 (2006).
- [104] A. Guerfi, M. Dontigny, P. Charest, M. Petitclerc, M. Lagacé, A. Vijh, and K. Zaghib, *Journal of Power Sources* **195**, 845 (2010).
- [105] L. J. Hardwick, M. Holzapfel, and A. Wokaun, *Journal of Raman Spectroscopy* **38**, 110 (2007).

- [106] C. Hardacre, J. D. Holbrey, S. E. J. McMath, D. T. Bowron, and A. K. Soper, *J. Chem. Phys.* **118**, 273 (2003).
- [107] C. Hardacre, S. E. J. McMath, M. Nieuwenhuyzen, D. T. Bowron, and A. K. Soper, *J. Phys.: Condens. Matter* **15**, S159 (2002).
- [108] H. V. R. Annapureddy, H. K. Kashyap, P. M. De Biase, and C. J. Margulis, *J. Phys. Chem. B* **114**, 16838 (2010).
- [109] L. Aguilera, S. Xiong, J. Scheers, and A. Matic, *Journal of Molecular Liquids* **210, Part B IS -**, 238 (2015).
- [110] K. Ueno, R. Tatara, S. Tsuzuki, S. Saito, H. Doi, K. Yoshida, T. Mandai, M. Matsugami, Y. Umebayashi, K. Dokko, and M. Watanabe, *Phys. Chem. Chem. Phys.* **17**, 8248 (2015).
- [111] C. Hardacre, J. D. Holbrey, C. L. Mullan, T. G. A. Youngs, and D. T. Bowron, *J. Chem. Phys.* **133**, 074510 (2010).
- [112] A. Triolo, O. Russina, B. Fazio, G. B. Appetecchi, M. Carewska, and S. Passerini, *J. Chem. Phys.* **130**, 164521 (2009).
- [113] S. Patra and A. Samanta, *J. Phys. Chem. B* **116**, 12275 (2012).
- [114] H. K. Kashyap, C. S. Santos, R. P. Daly, J. J. Hettige, N. S. Murthy, H. Shirota, E. W. Castner, and C. J. Margulis, *J. Phys. Chem. B* **117**, 1130 (2013).
- [115] H. K. Kashyap, C. S. Santos, N. S. Murthy, J. J. Hettige, K. Kerr, S. Ramati, J. Gwon, M. Gohdo, S. I. Lall-Ramnarine, J. F. Wishart, C. J. Margulis, and E. W. Castner, *J. Phys. Chem. B* **117**, 15328 (2013).
- [116] S. Li, J. L. Bañuelos, J. Guo, L. Anovitz, G. Rother, R. W. Shaw, P. C. Hillesheim, S. Dai, G. A. Baker, and P. T. Cummings, *J. Phys. Chem. Lett.* **3**, 125 (2011).
- [117] S. M. Urahata and M. C. C. Ribeiro, *J. Phys. Chem. Lett.* **1**, 1738 (2010).
- [118] B. L. Bhargava, R. Devane, M. L. Klein, and S. Balasubramanian, *Soft Matter* **3**, 1395 (2007).
- [119] A. Martinelli, M. Maréchal, Å. Östlund, and J. Camedouzou, *Phys. Chem. Chem. Phys.* **15**, 5510 (2013).
- [120] A. Triolo, O. Russina, B. Fazio, R. Triolo, and E. Di Cola, *Chemical Physics Letters* **457**, 362 (1999).
- [121] M. Kofu, M. Nagao, T. Ueki, Y. Kitazawa, Y. Nakamura, S. Sawamura, M. Watanabe, and O. Yamamuro, *J. Phys. Chem. B* **117**, 2773 (2013).
- [122] K. Binnemans, *Chem. Rev.* **105**, 4148 (2005).
- [123] C. A. Angell, *Chem. Rev.* **90**, 523 (1990).
- [124] C. A. Angell, *Science* **267**, 1924 (1995).
- [125] M. D. Ediger, C. A. Angell, and S. R. Nagel, *The Journal of Physical ...* **100**, 13200 (1996).
- [126] I. Nicotera, C. Oliviero, W. A. Henderson, G. B. Appetecchi, and S. Passerini, *J. Phys. Chem. B* **109**, 22814 (2005).
- [127] J. C. Araque, J. J. Hettige, and C. J. Margulis, *J. Phys. Chem. B* **119**, 12727 (2015).
- [128] M. Kofu, M. Tyagi, Y. Inamura, K. Miyazaki, and O. Yamamuro, *The Journal of Chemical Physics* **143**, 234502 (2015).
- [129] O. Yamamuro, T. Yamada, M. Kofu, M. Nakakoshi, and M. Nagao, *J. Chem. Phys.* **135**, 054508 (2011).
- [130] P. Gabbott, Blackwell Publishing Ltd (2008).
- [131] G. Höhne, W. F. Hemminger, and H. J. Flammersheim, Springer (2003).
- [132] P. J. Haines, The Royal Society of Chemistry (2002).

- [133] F. Kremer and A. S. nhals, *Broadband Dielectric Spectroscopy* (Springer, 2003).
- [134] F. J. Boerio and J. L. Koenig, *J. Polym. Sci. B Polym. Phys.* **7**, 1489 (1969).
- [135] C. V. Raman and K. S. Krishnan, *Nature* **121**, 501 (1928).
- [136] *Naturwissenschaften* **16**, 557 (1928).
- [137] A. Smekal, *Naturwissenschaften* **11**, 873 (1923).
- [138] D. A. Long, *The Raman Effect* (Frank Cass (UK), 2002).
- [139] R. L. McCreery, *Raman Spectroscopy for Chemical Analysis* (John Wiley & Sons, 2005).
- [140] D. J. Gardiner, *Practical Raman Spectroscopy* (Springer Verlag, 1989).
- [141] E. E. Whiting, *Journal of Quantitative Spectroscopy and Radiative Transfer* **8**, 1379 (1968).
- [142] S. R. Drayson, *Journal of Quantitative Spectroscopy and Radiative Transfer* **16**, 611 (1976).
- [143] B. H. Armstrong, *Journal of Quantitative Spectroscopy and Radiative Transfer* **7**, 61 (1967).
- [144] F. Schreier, *Journal of Quantitative Spectroscopy and Radiative Transfer* **48**, 743 (1992).
- [145] J. Humlíček, *Journal of Quantitative Spectroscopy and Radiative Transfer* **27**, 437 (1982).
- [146] O. Glatter and O. Kratky, **102**, (1982).
- [147] A. Labrador, Y. Cerenius, C. Svensson, K. Theodor, and T. Plivelic, *J. Phys.: Conf. Ser.* **425**, 072019 (2013).